Vertically and horizontally polarized diffuse double-scatter cross sections of one-dimensional random rough surfaces that exhibit enhanced-backscatter–full-wave solutions

E. Bahar and M. El-Shenawee

Department of Electrical Engineering/Center for Electro-Optics, University of Nebraska, Lincoln, Nebraska 68588-0511

Received August 13, 1993; revised manuscript received February 10, 1994; accepted March 9, 1994

Full-wave solutions for the vertically and horizontally polarized diffuse single- and double-scatter cross sections of random rough surfaces are given in terms of multidimensional integral expressions. The one-dimensional random rough surface is characterized by joint probability-density functions for the surface heights and slopes, and we account for the correlations between the surface heights and slopes. The full-wave solutions are compared with experimental results. The sharp enhanced backscatter is due to the contributions associated with the quasi-antiparallel paths in the expression for the double-scatter cross section. We conduct a comprehensive parametric study to determine the dependence of the level and the angular width of the sharp enhanced backscatter on the rough-surface characteristics. The results for the diffuse double-scatter cross sections exhibit a distinct dependence on polarization. Full-wave, high-frequency approximations that are practically independent of polarization provide useful physical insights into the problem.

1. INTRODUCTION

Enhanced backscatter from rough surfaces has been observed in numerous carefully conducted experiments.[1–5] Even though the original observations of backscatter enhancement were conducted with two-dimensional rough surfaces,[1,2] no numerical or analytical solutions for the scattered electromagnetic fields were available. Thus it was not possible to conduct a comprehensive parametric study of the observed phenomena and to interpret them physically. More recently, experimental, numerical, and analytical investigations have been conducted with surfaces that are essentially rough in only one dimension.[3–5] The plane of incidence is restricted to the plane in which the local normal to the rough surfaces lies. Thus these one-dimensional rough surfaces do not depolarize the incident waves, and the problem is essentially scalar. While one-dimensional rough surfaces do not have the same range of physical applications as do two-dimensional rough surfaces, the numerical and analytical solutions to the electromagnetic scattering problem for one-dimensional rough surfaces are significantly easier to solve (both analytically and numerically).

The full-wave solutions are based on the complete spectral expansion of the scattered fields and the imposition of exact boundary conditions. Maxwell's equations are converted into generalized telegraphist's equations that are solved iteratively. The analytical solutions for the near fields and the far fields include the primary fields as well as the diffuse single- and double-scatter fields. They are expressed in a form that can be solved numerically in a tractable manner. The basis for this analysis is the full-wave solutions for the double-scatter far fields from one–dimensional (deterministic) surfaces. They can be expressed as three-dimensional integrals (not integral equations) over two spatial coordinate variables and one wave-vector variable.[6–9] Using these integral expressions, we can formally express the mean (expected) value of the scatter cross sections (intensities) as 14-dimensional integrals involving four spatial variables, two wave-vector variables, and eight random variables representing the surface heights and the surface slopes at four points on the rough surface. Since the full-wave surface element scattering coefficients are slope dependent, it is necessary to account for height/slope correlations.[10] After several physically justifiable approximations are introduced, these fourteen-dimensional integrals are reduced to six-dimensional integrals. These analytical solutions have readily interpretable forms that involve the evaluation of two single-scatter cross sections and the interaction between them through the scatter wave vectors. However, they are still not in a form that can be evaluated rapidly, even by supercomputers. Further transformations of the integrand permit the evaluation of these six-dimensional integrals essentially as three-dimensional integrals. These transformed six-dimensional integral expressions can be readily evaluated.

In earlier studies[11–13] the high-frequency (stationary-phase physical optics) approximations were used to reduce the six-dimensional integral expressions into two-dimensional integral expressions. The high-frequency (stationary-phase) approximations for the double-scatter cross sections are practically independent of polarization, and the angular width of the sharp enhanced backscatter is significantly reduced. However, the stationary-phase approximations provide useful insights into the physical nature of the problem and into its numerical solution in a tractable manner.

0740-3232/94/082271-15$06.00

Enhanced backscatter is observed from rough surfaces with large root-mean-square heights that are only a fraction of the electromagnetic wavelength, provided that the mean-square slopes are large ($\langle h_x^2 \rangle \geq 0.5$). These rough-surface structures could be used in the design of road signs and aerodynamic targets (decoys) that exhibit enhanced backscatter. We have conducted a parametric study to determine the effects of varying the statistical parameters of the rough surface (root-mean-square height, slope, and correlation length) on the enhanced backscattered intensities. The random rough surface is characterized by joint surface height/slope probability-density functions at two pairs of points on the surface (including the rough-surface height autocorrelation function or its Fourier transform, the surface height spectral density function).[10] The effects of varying the incident angle, the polarization of the electromagnetic waves, and the rough-surface parameters are also studied. The results are compared with recently published experimental results. Similarities and differences between the full-wave approach and other solutions are also discussed.

2. FORMULATION OF THE PROBLEM

For suppressed $\exp(j\omega t)$ time excitations the full-wave solutions for the diffuse single-scatter near fields $G_s^{fP}(\mathbf{r})$ from one-dimensional rough surfaces $[y = h(x)]$ (Refs. 6–9) are (see Appendix A)

$$G_s^{fP}(\mathbf{r}) = \frac{-k_0}{2\pi} \int_{n_y'=-\infty}^{\infty} \int_{x_s=-L}^{L} \frac{D^P(\hat{n}', \hat{n}^i)}{-n_y^i + n_y'} \times \exp[-jk_0(\hat{n}' \cdot \mathbf{r})]\{\exp[-jk_0 \mathbf{r}_s \cdot (\hat{n}^i - \hat{n}')] - \exp[-jk_0 \mathbf{r}_t \cdot (\hat{n}^i - \hat{n}')]\} \times U(\hat{r}_s) \mathrm{d}x_s \frac{\mathrm{d}n_y'}{[1 - (n_y')^2]^{1/2}} G^{iP}(0), \quad (1)$$

where $\hat{n}^i$ is the unit vector in the direction of the incident fields,

$$\hat{n}^i = n_x^i \hat{a}_x + n_y^i \hat{a}_y . \quad (2a)$$

The unit vectors $\hat{a}_x$ and $\hat{a}_y$ are along the x and y axes, respectively, and the unit vector $\hat{a}_y$ is normal to the mean plane of the rough surface ($y = 0$). The wave vector in the direction of the fields scattered from the surface is

$$\hat{n}' = n_x' \hat{a}_x + n_y' \hat{a}_y . \quad (2b)$$

For propagating waves the limits of the wave-vector variable n_y' are $(-1, 1)$. The variable $n_x' = +[1 - (n_y')^2]^{1/2}$ for $x - x_s > 0$ and $-[1 - (n_y')^2]^{1/2}$ for $x - x_s < 0$.[14] Note that in Eq. (1) the denominator $[1 - (n_y')^2]^{1/2}$ is always positive (even when n_x' changes sign).[15,16] The position vector to the observer is $\mathbf{r}$, while the position vector to any point on the rough surface is $\mathbf{r}_s$ and its projection on the mean plane $y = 0$ is $\mathbf{r}_t$:

$$\mathbf{r} = x\hat{a}_x + y\hat{a}_y, \qquad \mathbf{r}_s = x_s \hat{a}_x + h(x_s)\hat{a}_y, \qquad \mathbf{r}_t = x_s \hat{a}_x . \quad (3)$$

For high frequencies the shadow function $U(\mathbf{r}_s)$ is equal to unity if the point on the surface is illuminated by the incident waves and visible at the receiver.[17,18] The free-space wave number is $k_0 = \omega(\mu_0 \epsilon_0)^{1/2}$. In Eq. (1) the superscript denotes the polarization of the incident and scatter waves, $P = V$ (vertical) and H (horizontal). The vertically and horizontally polarized incident plane-wave amplitudes at the origin are $G^{iP}(0)$. The length of the perturbed rough surface is $2L$. The slope-dependent surface element scattering coefficient at point $\mathbf{r}_s$ on the surface is $D^P(\hat{n}', \hat{n}^i)$.[19] The scattering coefficient depends on the polarizations of the incident and scattered waves, the media on both sides of the rough interface, and the local normal $\hat{n}$ on the rough surface[6] (see Appendix A).

We use the full-wave expression (1) to determine the differential wave-vector contribution to the diffuse single-scatter field, $\mathrm{d}G_2(\mathbf{r}_{s2}')$, incident on the rough surface at $\mathbf{r}_{s2}'$ ($\mathbf{r}_s \rightarrow \mathbf{r}_{s1}'$ and $\mathbf{r} \rightarrow \mathbf{r}_{s2}'$; see Fig. 1). Thus

$$\mathrm{d}G_2^{fP}(\mathbf{r}_{s2}') = \frac{-k_0}{2\pi} \int_{x_{s1}'=L}^{L} \frac{D_{1'}^P(\hat{n}', \hat{n}^i}{-n_y^i + n_y'} \exp(-jk_0 \hat{n}' \cdot \mathbf{r}_{s2}') \times \exp[jk_0 x_{s1}'(n_x' - n_x^i)] \times \{\exp[jk_0 h(x_{s1}')(n_y' - n_y^i)] - 1\} \times U(\mathbf{r}_{s1}')\mathrm{d}x_{s1}' \frac{\mathrm{d}n_y'}{[1 - (n_y')^2]^{1/2}} G^{iP}(0), \quad (4)$$

where the position vectors to points $1'$ and $2'$ on the rough surface are given by $\mathbf{r}_{s1}'$ and $\mathbf{r}_{s2}'$ (see Fig. 1):

$$\mathbf{r}_{s1}' = x_{s1}' \hat{a}_x + h(x_{s1}')\hat{a}_y, \qquad \mathbf{r}_{s2}' = x_{s2}' \hat{a}_x + h(x_{s2}')\hat{a}_y . \quad (5)$$

The full-wave solution for the differential wave-vector contribution to the double-scatter fields, $\mathrm{d}G_d^{fP}(\mathbf{r})$, is obtained from Eq. (1) if we replace $G^{iP}(0)$ by $\mathrm{d}G_2^{fP}(0)$ as follows:

$$\mathrm{d}G_d^{fP}(\mathbf{r}) = \frac{-k_0}{2\pi} \int_{n_y''=-\infty}^{\infty} \int_{x_{s2}'=-L}^{L} \frac{D_{2'}^P(\hat{n}'', \hat{n}')}{n_y'' - n_y'} \times \exp[-jk_0(\hat{n}'' \cdot \mathbf{r})]\{\exp[-jk_0 \mathbf{r}_{s2}' \cdot (\hat{n}' - \hat{n}'')] - \exp[-jk_0 \mathbf{r}_{t2} \cdot (\hat{n}' - \hat{n}'')]\} \times U(\mathbf{r}_{s2}')\mathrm{d}x_{s2}' \frac{\mathrm{d}n_y''}{[1 - (n_y'')^2]^{1/2}} \mathrm{d}G_2^{fP}(0). \quad (6a)$$

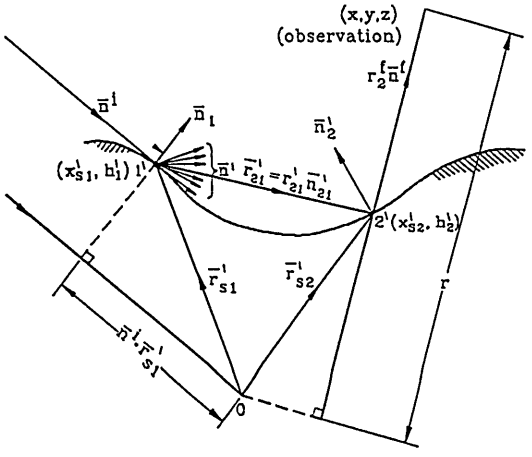

Fig. 1. Double-scatter electromagnetic waves.

If we use the steepest-descent method to integrate Eq. (6a) with respect to n_y'', the far-field expression for the differential wave-vector contribution to the double-scatter diffuse field is obtained. On substituting for $dG_2^{fp}(0)$, using Eq. (4), and integrating over the wave-vector spectrum $n_y' = \hat{n}' \cdot \hat{a}_y$ (see Fig. 1), we obtain the expression for the double-scatter diffuse far field[6–9]:

$$
\begin{aligned}
&G_d^{fP}(\mathbf{r}) \\
&= \frac{k_0^4}{4\pi^2}\left(\frac{2\pi}{k_0 r}\right)^{1/2} \exp(j\pi/4)\exp(-jk_0 r) \\
&\times \int_{n_{y'}=-1}^{1} \int_{x_{s1'}=-L}^{L} \int_{x_{s2'}=-L}^{L} \frac{D_{1'}^{P}(\hat{n}', \hat{n}^i) D_{2'}^{P}(\hat{n}^f, \hat{n}')}{[k_0(-n_y^i + n_y')][k_0(n_y^f - n_y')]} \\
&\times \exp[-jk_0 x_{s1'}(n_x^i - n_x')]\exp[jk_0 x_{s2'}(n_x^f - n_x')] \\
&\times \{\exp[-jk_0 h(x_{s1'})(n_y^i - n_y')] - 1\} \\
&\times \{\exp[jk_0 h(x_{s2'})(n_y^f - n_y')] - 1\} \\
&\times U(\mathbf{r}_{s1'})U(\mathbf{r}_{s2'})\,dx_{s2'}\,dx_{s1'}\,\frac{dn_y'}{[1-(n_y')^2]^{1/2}}\,G^{iP}(0). \qquad (6b)
\end{aligned}
$$

Note that the wave vector $\mathbf{k}_0' = k_0\hat{n}'$ is in the direction of the fields scattered from the surface at $\mathbf{r}_{s1}'$ to the surface at $\mathbf{r}_{s2}'$ (see Fig. 1). The slope-dependent surface element scattering coefficients at points $\mathbf{r}_{s1}'$ and $\mathbf{r}_{s2}'$ on the surface are $D_{1'}^{P}(\hat{n}', \hat{n}^i)$ and $D_{2'}^{P}(\hat{n}^f, \hat{n}')$, respectively. The local unit vectors normal at these points to the surface are $\hat{n}_{1'}$ and $\hat{n}_{2'}$. For high frequencies the shadow function $U(\mathbf{r}_{s1}')$ is equal to unity if the point at $\mathbf{r}_{s1}'$ is illuminated by the incident waves $(\hat{n}^i)$ and visible at point $\mathbf{r}_{s2}'$. The shadow function $U(\mathbf{r}_{s2}')$ is equal to unity if the point at $\mathbf{r}_{s2}'$ is illuminated by a source at $\mathbf{r}_{s1}'$ and visible at the receiver $(\hat{n}^f)$.[17]

The integrand of the diffuse double-scatter field expression given by Eq. (6b) is not singular. The reason is that, as $k_0(-n_y^i + n_y') \to 0$ or as $k_0(n_y^f - n_y') \to 0$, the numerator in the integrand of Eq. (6b) is also proportional to $k_0(-n_y^i + n_y')$ or to $k_0(n_y^f - n_y')$ (see Appendix A). Equation (6b) does not contain the zero-order term.[20]

In the neighborhood of a rough-surface element that contributes significantly to single scatter, the familiar stationary-phase condition for the integrand of Eq. (1) prevails. Thus the vector normal to the rough surface at a stationary phase (specular) point is along the direction of the bisector $\hat{n}^f - \hat{n}^i$. For significant contributions to double scatter to occur in the neighborhood of a pair of surface elements at $\mathbf{r}_{s1}$ and $\mathbf{r}_{s2}$, the corresponding stationary-phase condition for the integrand of Eq. (6b) must prevail.[6] In this case the vectors normal to the surface at $\mathbf{r}_{s1}$ and $\mathbf{r}_{s2}$ must be simultaneously along the bisectors $\hat{n}_{21} - \hat{n}^i$ and $\hat{n}^f - \hat{n}_{21}$, where $\hat{n}_{21}$ is the unit vector in the direction $\mathbf{r}_{s2} - \mathbf{r}_{s1}$.

The double-scatter intensity is obtained by multiplication of expressions for the field (6b) by its complex conjugate $G_d^{fP*}(\mathbf{r})$. To distinguish the conjugate from the field expression, we denote the position-vector and wave-vector variables by a double prime instead of a single prime. Thus $\mathbf{k}_0'' = k_0\hat{n}''$ is the wave vector in the direction of the conjugate scattered fields from a point on the surface at $\mathbf{r}_{s1}''$ to a point on the surface at $\mathbf{r}_{s2}''$ (see Fig. 2). It is given by

$$
\mathbf{k}_0'' = k_0\hat{n}'' = k_0(n_x''\hat{a}_x + n_y''\hat{a}_y), \qquad (7)
$$

and the position vectors are

$$
\mathbf{r}_{s1}'' = x_{s1}''\hat{a}_x + h(x_{s1}'')\hat{a}_y, \qquad \mathbf{r}_{s2}'' = x_{s2}''\hat{a}_x + h(x_{s2}'')\hat{a}_y. \qquad (8)
$$

The radar cross section for a one-dimensional random rough surface is defined as

$$
\sigma = \frac{2\pi r}{2L}\,\frac{G_d^{fP}(\mathbf{r})G_d^{fP*}(\mathbf{r})}{G^{iP}(0)G^{iP*}(0)}. \qquad (9)
$$

Thus, using Eq. (6b) and the corresponding expression for its complex conjugate, we can express the statistical average of the diffuse double-scatter radar cross section, denoted by $\langle\sigma_d\rangle$, as

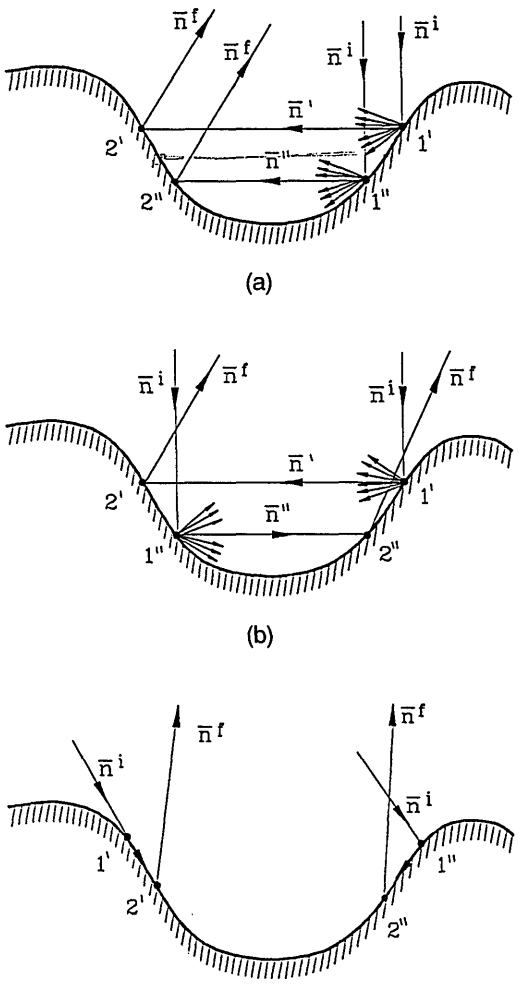

Fig. 2. (a) Quasi-parallel, regular path ($\hat{n}' \approx \hat{n}''$), (b) quasi-antiparallel, cross path ($\hat{n}' \approx -\hat{n}''$), and (c) insignificant contributions when $\mathbf{r}_{s1}' \to \mathbf{r}_{s2}'$ and $\mathbf{r}_{s1}'' \to \mathbf{r}_{s2}''$, since $D \to 0$.

$$\langle \sigma_d \rangle = \frac{k_0^7}{4\pi^2}\frac{1}{2L} \times \int_{n_y''=-1}^{1}\int_{n_y'=-1}^{1}\int_{x_{s1}'=-L}^{L}\int_{x_{s2}'=-L}^{L}\int_{x_{s1}''=-L}^{L}\int_{x_{s2}''=-L}^{L} \left\langle \frac{D_{2'}^{P}(\hat{n}^f,\hat{n}')D_{1'}^{P}(\hat{n}',\hat{n}^i)D_{2''}^{P*}(\hat{n}^f,\hat{n}'')D_{1''}^{P*}(\hat{n}'',\hat{n}^i)}{[k_0(-n_y^i+n_y')][k_0(n_y^i-n_y'')][k_0(n_y^f-n_y')][k_0(-n_y^f+n_y'')]} \times \{\exp[-jk_0h(x_{s1}')(n_y^i-n_y')]-1\}\{\exp[jk_0h(x_{s2}')(n_y^f-n_y')]-1\} \times \{\exp[jk_0h(x_{s1}'')(n_y^i-n_y'')]-1\}\{\exp[-jk_0h(x_{s2}'')(n_y^f-n_y'')]-1\}U(\mathbf{r}_{s1}')U(\mathbf{r}_{s2}')U(\mathbf{r}_{s1}'')U(\mathbf{r}_{s2}'')\right\rangle \times \exp\{jk_0[n_x^f(x_{s2}'-x_{s2}'')-n_x^i(x_{s1}'-x_{s1}'')-n_x'(x_{s2}'-x_{s1}')+(n_x''(x_{s2}''-x_{s1}'')]\} \times dx_{s2}''dx_{s1}''dx_{s2}'dx_{s1}'\frac{dn_y'}{[1-(n_y')^2]^{1/2}}\frac{dn_y''}{[1-(n_y'')^2]^{1/2}}. \tag{10}$$

In Eq. (10) the random variables are the heights and the slopes (contained in the scattering coefficients) of the rough surface at points 1′, 2′, 1″, and 2″. For a random rough surface the shadow functions $U(\mathbf{r}_{s1}')$, $U(\mathbf{r}_{s2}')$, $U(\mathbf{r}_{s1}'')$, and $U(\mathbf{r}_{s2}'')$ are given by Sancer.[17] The statistical average of the intensities with respect to the random heights and slopes at two pairs of points on the surface involves the conditional joint characteristic functions.[10]

The significant contributions to the double-scatter intensities are shown to come from two combinations of double-scatter paths (mechanisms)[21–24] [see Figs. 2(a) and 2(b)]. In this manuscript they are referred to as quasi-parallel ($\hat{n}' \approx \hat{n}''$), regular path [see Fig. 2(a)] and quasi-antiparallel ($\hat{n}' \approx -\hat{n}''$), cross path [see Fig. 2(b)]. The incoherent diffuse double-scatter intensity is the sum of contributions from the quasi-parallel and quasi-antiparallel paths.[11–13,25]

For the typical quasi-parallel (regular) path [see Fig. 2(a)] the variables of integration in Eq. (10) are changed from x_{s1}', x_{s2}', x_{s1}'', and x_{s2}'' to x_{d1}, x_{d2}, x_{c1}, and x_{c2}, where

$$x_{d1} = x_{s1}' - x_{s1}'', \qquad x_{d2} = x_{s2}' - x_{s2}'', \tag{11a}$$

$$x_{c1} = \frac{x_{s1}' + x_{s1}''}{2}, \qquad x_{c2} = \frac{x_{s2}' + x_{s2}''}{2}. \tag{11b}$$

The region of integration for x_{d1} and x_{c1} (or x_{d2} and x_{c2}) is diamond shaped with end points at $\pm 2L$ and $\pm L$, respectively. Thus Eq. (10) can be expressed as

$$\langle \sigma_d \rangle = \frac{k_0^7}{4\pi^2}\frac{1}{2L} \times \int_{n_y''=-1}^{1}\int_{n_y'=-1}^{1}\int_{x_{d1},x_{d2},x_{c1},x_{c2}} \left\langle \frac{D_{2'}^{P}(\hat{n}^f,\hat{n}')D_{1'}^{P}(\hat{n}',\hat{n}^i)D_{2''}^{P*}(\hat{n}^f,\hat{n}'')D_{1''}^{P*}(\hat{n}'',\hat{n}^i)}{[k_0(-n_y^i+n_y')][k_0(n_y^i-n_y'')][k_0(n_y^f-n_y')][k_0(-n_y^f+n_y'')]} \times \{\exp[-jk_0h(x_{s1}')(n_y^i-n_y')]-1\}\{\exp[jk_0h(x_{s2}')(n_y^f-n_y')]-1\} \times \{\exp[jk_0h(x_{s1}'')(n_y^i-n_y'')]-1\}\{\exp[-jk_0h(x_{s2}'')(n_y^f-n_y'')]-1\}U(\mathbf{r}_{s1}')U(\mathbf{r}_{s2}')U(\mathbf{r}_{s1}'')U(\mathbf{r}_{s2}'')\right\rangle \times \exp\left(jk_0\left\{ x_{d1}\left[-n_x^i + \left(\frac{n_x' + n_x''}{2}\right)\right] + x_{d2}\left[n_x^f - \left(\frac{n_x' + n_x''}{2}\right)\right] + x_{c1}(n_x' - n_x'') + x_{c2}(-n_x' + n_x'')\right\}\right) \times dx_{d1}dx_{d2}dx_{c1}dx_{c2}\frac{dn_y'}{[1-(n_y')^2]^{1/2}}\frac{dn_y'}{[1-(n_y'')^2]^{1/2}}. \tag{12}$$

It is shown[6] that, for a typical (sinusoidal) surface depression (valley), there are four distinct paths that contribute significantly to the double-scatter fields for zero incident and scatter angles. Two correspond to $n_x' = [1-(n_y')^2]^{1/2}$, and two correspond to $n_x' = -[1-(n_y')^2]^{1/2}$. One pair is above and one pair is below the level where the surface slope is stationary and the curvature of the surface changes sign. In general, there could be more than two quasi-parallel and quasi-antiparallel pairs of paths on the average, depending on the mean radii of curvature of the rough surfaces and therefore on the small-scale roughness of the rough surfaces. This explains why the observed backscatter enhancement increases significantly as the small-scale content of the rough-surface spatial spectrum increases.[26]

The corresponding expression for the coherent cross section $\langle \sigma_c \rangle$ is obtained from Eq. (12) on the assumption that all the height and slope random variables are uncorrelated. For convenience, the incoherent cross section (which is the difference between $\langle \sigma_d \rangle$ and $\langle \sigma_c \rangle$) is evaluated. Thus, provided that $2L$ is much larger than the correlation length l_c, for purposes of evaluating the incoherent diffuse scatter cross sections the limits of x_{d1} and x_{d2} can be assumed to be $(-\infty, \infty)$ whereas the limits of x_{c1} and x_{c2} are $(-L, L)$.[27]

The random variables in Eq. (12) are the heights $h_1' = h(x_{s1}')$, $h_1'' = h(x_{s1}'')$, $h_2' = h(x_{s2}')$, and $h_2'' = h(x_{s2}'')$, the slopes h_{x1}', h_{x1}'', h_{x2}', and h_{x2}'', and the shadow functions $U(\mathbf{r}_{s1}')$, $U(\mathbf{r}_{s2}')$, $U(\mathbf{r}_{s1}'')$, and $U(\mathbf{r}_{s2}'')$ at points 1′, 1″, 2′, and 2″ on the rough surface [see Figs. 2(a) and 2(b)].

Assuming that $k_0\rho \gg 1$ (where ρ is the radius of curvature), the slope-dependent scattering coefficients D^P in Eq. (12) are expanded about their values at the midpoints x_{c1} and x_{c2}. Thus, for example,

$$D_{1'}{}^{P}(\hat{n}', \hat{n}^i) = D^P(\hat{n}', \hat{n}^i)|_{h_{x1'}=h_{x1c}} + k_0(x_{s1}' - x_{c1}) \times \frac{\partial D^P(\hat{n}', \hat{n}^i)}{\partial k_0 x_{s1}'}\bigg|_{x_{s1}'=x_{c1}} + \cdots$$
$$= D^P(\hat{n}', \hat{n}^i)|_{h_{x1'}=h_{x1c}} + k_0(x_{s1}' - x_{c1}) \times \left[\frac{\partial D^P(\hat{n}', \hat{n}^i)}{\partial h_{x1}'}\frac{\partial h_{x1}'}{\partial k_0 x_{s1}'}\right]_{x_{s1}'=x_{c1}} + \cdots \quad (13)$$

On assuming small curvature (large radii of curvature), the higher-order terms proportional to the first- and higher-order derivatives of $h(x, z)$ (Refs. 17 and 28) are ignored. Thus the scattering coefficients are approximated by their values at the midpoints x_{c1} and x_{c2}. Substituting Eq. (13) into Eq. (12), we obtain

$$p[h_1', h_1'', h_2', h_2'', h_{x1c}, h_{x2c}, U(\mathbf{r}_{s1}'), U(\mathbf{r}_{s2}'), U(\mathbf{r}_{s1}''), U(\mathbf{r}_{s2}'')]$$
$$= p(h_1', h_1'' \mid h_{x1c})p(h_{x1c})p(h_2', h_2'' \mid h_{x2c})p(h_{x2c}) \times p[U(\mathbf{r}_{s1}'), U(\mathbf{r}_{s1}'')]p[U(\mathbf{r}_{s2}'), U(\mathbf{r}_{s2}'')], \quad (15)$$

where the heights at the pair of points $1'$, $1''$ are assumed to be statistically independent of the heights at the pair of points $2'$, $2''$ for the quasi-parallel double-scatter paths.[22] If point $1'$ approaches point $2'$ and/or if point $1''$ approaches point $2''$, the integrand vanishes, since the scattering coefficients D^P become vanishingly small[6] [see Fig. 2(c)]. On substituting Eq. (15) into Eq. (14) and integrating with respect to the shadow functions $U(\mathbf{r}_{s1}')$, $U(\mathbf{r}_{s2}')$, $U(\mathbf{r}_{s1}'')$, and $U(\mathbf{r}_{s2}'')$,[17] one obtains

$$\langle\sigma_d\rangle = \frac{k_0{}^7}{4\pi^2 2L} \times \int_{n_y''=-1}^{1}\int_{n_y'=-1}^{1}\int_{x_{d1}=-\infty}^{\infty}\int_{x_{d2}=-\infty}^{\infty}\int_{x_{c1}=-L}^{L}\int_{x_{c2}=-L}^{L}\Bigg\langle \frac{[D^P(\hat{n}^f, \hat{n}')D^{P*}(\hat{n}^f, \hat{n}'')]_{h_{x2'}=h_{x2''}=h_{x2c}}[D^P(\hat{n}', \hat{n}^i)D^{P*}(\hat{n}'', \hat{n}^i)]_{h_{x1'}=h_{x1''}=h_{x1c}}}{[k_0(-n_y^i + n_y')][k_0(n_y^i - n_y'')][k_0(n_y^f - n_y')][k_0(-n_y^f + n_y'')]}$$
$$\times \{\exp[-jk_0h(x_{s1}')(n_y^i - n_y')] - 1\}\{\exp[jk_0h(x_{s2}')(n_y^f - n_y')] - 1\}$$
$$\times \{\exp[jk_0h(x_{s1}'')(n_y^i - n_y'')] - 1\}\{\exp[-jk_0h(x_{s2}'')(n_y^f - n_y'')] - 1\}U(\mathbf{r}_{s1}')U(\mathbf{r}_{s2}')U(\mathbf{r}_{s1}'')U(\mathbf{r}_{s2}'')\Bigg\rangle$$
$$\times \exp\left\{jk_0x_{d1}\left[-n_x{}^i + \left(\frac{n_x' + n_x''}{2}\right)\right]\right\}\exp\left\{jk_0x_{d2}\left[n_x{}^f - \left(\frac{n_x' + n_x''}{2}\right)\right]\right\}\exp\{jk_0[x_{c1}(n_x' - n_x'') + x_{c2}(-n_x' + n_x'')\}$$
$$\times dx_{c2}dx_{c1}dx_{d2}dx_{d1}\frac{dn_y'}{[1 - (n_y')^2]^{1/2}}\frac{dn_y''}{[1 - (n_y'')^2]^{1/2}}. \quad (14)$$

$$\langle\sigma_d\rangle = \frac{k_0{}^7}{4\pi^2 2L}P(\hat{n}^i)P(\hat{n}^f) \times \int_{n_y', n_y''=-1}^{1}\int_{x_{c1}, x_{c2}=-L}^{L}\int_{x_{d1}, x_{d2}=-\infty}^{\infty}\int_{h_{x1c}, h_{x2c}=-\infty}^{\infty}\int_{h_1', h_1'', h_2', h_2''=-\infty}^{\infty}\frac{[D(\hat{n}^f, \hat{n}')D^*(\hat{n}^f, \hat{n}'')]_{h_{x2'}=h_{x2''}=h_{x2c}}[D(\hat{n}', \hat{n}^i)D^*(\hat{n}'', \hat{n}^i)]_{h_{x1'}=h_{x1''}=h_{x1c}}}{[k_0(-n_y^i + n_y')][k_0(n_y^i - n_y'')][k_0(n_y^f - n_y')][k_0(-n_y^f + n_y'')]}$$
$$\times \{\exp[-jk_0h_1'(n_y^i - n_y')] - 1\}\{\exp[jk_0h_2'(n_y^f - n_y')] - 1\}\{\exp[jk_0h_1''(n_y^i - n_y'')] - 1\}\{\exp[-jk_0h_2''(n_y^f - n_y'')] - 1\}$$
$$\times p(h_1', h_1'' \mid h_{x1c})p(h_2', h_2'' \mid h_{x2c})p(h_{x1c})p(h_{x2c})[1 - P_2(|n_y'|)][1 - P_2(|n_y''|)]$$
$$\times \exp\left\{jk_0x_{d1}\left[-n_x{}^i + \left(\frac{n_x' + n_x''}{2}\right)\right]\right\}\exp\left\{jk_0x_{d2}\left[n_x{}^f - \left(\frac{n_x' + n_x''}{2}\right)\right]\right\}\exp\{jk_0[x_{c1}(n_x' - n_x'') + x_{c2}(-n_x' + n_x'')\}$$
$$\times dh_1'dh_1''dh_2'dh_2''dh_{x1c}dh_{x2c}dx_{d1}dx_{d2}dx_{c1}dx_{c2}\frac{dn_y'}{[1 - (n_y')^2]^{1/2}}\frac{dn_y''}{[1 - (n_y'')^2]^{1/2}}. \quad (16)$$

We reduced the number of random variables from 12 in Eq. (12) to 10 in Eq. (14) by approximating the slopes h_{x1}' and h_{x1}'' by h_{x1c} and the slopes h_{x2}' and h_{x2}'' by h_{x2c}. In Eq. (14) the random variables are the heights h_1', h_1'', h_2, and h_2'', the slopes h_{x1c} and h_{x2c}, and the shadow functions $U(\mathbf{r}_{s1}')$, $U(\mathbf{r}_{s2}')$, $U(\mathbf{r}_{s1}'')$, and $U(\mathbf{r}_{s2}'')$.

The rough surface is assumed to be characterized by a Gaussian joint probability-density function for the surface heights and slopes at two pairs of points on the surface. The surface height autocorrelation function and its Fourier transform (the rough-surface spectral density function) are also assumed here to be Gaussian. The full-wave analysis is not restricted to these assumptions. It can be applied to random surfaces characterized by any physical joint probability-density function and any physical spectral-density function.[29] For a quasi-parallel (regular) path the joint probability-density function for the random variables is approximated as

In Eq. (16) $P_2(|n_y'|)$ and $P_2(|n_y''|)$ (Ref. 17) are the probabilities that no parts of the surface intersect the scattered waves in the directions of the unit vectors $\hat{n}'$ and $\hat{n}''$, respectively[17,18] (see Appendix B). Thus $[1 - P_2(|n_y'|)] \times [1 - P_2(|n_y''|)]$ is the probability that the scattered fields in the direction of the unit vectors $\hat{n}'$ and $\hat{n}''$ intersect the surface. This product represents the shadow function probability for the multiple-scatter event. The probabilities that the surface does not shadow the incident and scattered waves are given in Eq. (16) by $P_2(\hat{n}^i)$ and $P_2(\hat{n}^f)$, respectively.[17,18] The probability-density functions for the slopes in Eq. (16) are given by $p(h_{x1c})$ and $p(h_{x2c})$, where h_{x1c} and h_{x2c} are the slopes at the midpoints x_{c1} and x_{c2} between $1'$ and $1''$ and between $2'$ and $2''$, respectively.

The rough surface is characterized by the following Gaussian joint probability-density function for the surface heights and slopes. In view of Ref. 10 it is expressed as

$$p_p(X) = p_{1p}(X_1)p_{2p}(X_2) = \frac{1}{(2\pi)^3}\prod_{n=1}^{2}\frac{1}{|P_{np}|^{1/2}}\exp\left(-\frac{1}{2}X_{np}{}^{T}P_{np}{}^{-1}X_{np}\right), \quad (17)$$

where P_{np} is the covariance matrix[10] (the subscript $n = 1, 2$, and p denotes the quasi-parallel case). For a quasi-parallel path the rough-surface height statistics at the pair of points $1'$, $1''$ and the pair of points $2'$, $2''$ are assumed to be uncorrelated[17] [see Fig. 2(a)]. The covariance matrix $P_{np}(x)$ for each pair of adjacent heights and midpoint slope is expressed as

$$P_{np}(X_{np}) = \begin{bmatrix} P_{11} & P_{12} \\ P_{21} & P_{22} \end{bmatrix}_{np}, \qquad X_{np} = \begin{pmatrix} h_n{}' \\ h_n{}'' \\ h_{xnc} \end{pmatrix}, \quad (18)$$

and $|P_{np}|$ is the determinant of P_{np}. In Eq. (18) P_{11}, P_{12}, P_{21}, and P_{22} are given by

$$[P_{11}]_{np} = \langle h^2\rangle\begin{bmatrix} 1 & R_n \\ R_n & 1 \end{bmatrix}, \quad (19a)$$

$$[P_{12}]_{np} = \begin{pmatrix} B_n \\ -B_n \end{pmatrix} = [P_{21}]_{np}{}^{T}, \quad (19b)$$

$$[P_{22}]_{np} = \langle h_x{}^2\rangle, \quad (19c)$$

where $[P_{21}]_{np}{}^{T}$ is the transpose of $[P_{21}]_{np}$. In Eq. (19) $\langle h^2\rangle$ is the mean-square height, and $\langle h_x{}^2\rangle$ is the mean-square slope. The correlations between the height at points $x_{s1}{}'$ and $x_{s1}{}''$ (or $x_{s2}{}'$ and $x_{s2}{}''$) and the slope at the midpoint x_{c1} (or x_{c2}) are given by $\pm B_1$ (or $\pm B_2$), and R_1 and R_2 are the surface height autocorrelation functions at these pairs of points. For the assumed Gaussian rough-surface spectral-density function the normalized surface height autocorrelation functions are

$$R_n = \exp[-(x_{dn}/l_c)^2], \quad (20)$$

where l_c is the correlation length of the rough surface and

$$B_n = \langle h_n{}' h_{xnc}\rangle = \frac{\langle h^2\rangle}{l_c{}^2}x_{dn}\exp[-(x_{dn}/2l_c)^2] = \langle h_x{}^2\rangle\frac{x_{dn}}{2}\exp[-(x_{dn}/2l_c)^2]. \quad (21)$$

The conditional joint characteristic functions for the pair of heights $h_n{}'$ and $h_n{}''$ given the midpoint slope h_{xnc} (the moment-generating function for multivariate normal probability-density functions) is given by[10,30]

$$\chi_{2n}(a_n, b_n \mid h_{xnc}) = \exp(jM_n{}^{T}S_n - {}^1\!/_2 S_n{}^{T}Z_nS_n), \quad (22)$$

where

$$M_n = h_{xnc}[P_{12}P_{22}{}^{-1}]_n, \quad (23a)$$

$$S_n = \begin{pmatrix} a_n \\ b_n \end{pmatrix}, \quad (23b)$$

$$Z_n = [P_{11} - P_{12}P_{22}{}^{-1}P_{21}]_n, \quad (23c)$$

$$a_1 = k_0(-n_y^i + n_y'), \qquad b_1 = k_0(n_y^i - n_y''),$$
$$a_2 = k_0(n_y^f - n_y'), \qquad b_2 = k_0(-n_y^f + n_y''). \quad (23d)$$

The moment-generating functions are given by[10,30]

$$\chi_{2n}(a_n, b_n \mid h_{xnc}) = \int_{h_n'=-\infty}^{\infty}\int_{h_n''=-\infty}^{\infty}\exp[j(a_nh_n{}' + b_nh_n{}'')] \times p(h_n', h_n'' \mid h_{xnc})\mathrm{d}h_n{}'\mathrm{d}h_n{}''. \quad (24)$$

Thus

$$\chi_{2n}(a_n, b_n \mid h_{xnc}) = \exp\left[jh_{xnc}\frac{B_n}{\langle h_x{}^2\rangle}(a_n - b_n)\right] \times \exp\left\{\left[\langle h^2\rangle(1 - R_n) - \frac{2B_n{}^2}{\langle h_x{}^2\rangle}\right]a_nb_n\right\} \times \exp\left[-\frac{1}{2}\left(\langle h^2\rangle - \frac{B_n{}^2}{\langle h_x{}^2\rangle}\right)(a_n + b_n)^2\right]. \quad (25)$$

On substituting Eq. (25) into Eq. (16), we can express the quasi-parallel diffuse double-scatter cross section $\langle\sigma_{pd}\rangle$ as the six-dimensional integral

$$\langle\sigma_{pd}\rangle = \frac{k_0{}^7}{4\pi^2 2L}P_2(\hat{n}^i)P_2(\hat{n}^f)\int_{n_y''=-1}^{1}\int_{n_y'=-1}^{1}\int_{x_{c1},x_{c2}=-L}^{L}\left(2\int_{x_{d1}=0}^{\infty}\int_{h_{x1c}=-\infty}^{\infty}\frac{[D(\hat{n}', \hat{n}^i)D^*(\hat{n}'', \hat{n}^i)]_{h_{x1}{}'=h_{x1}{}''=h_{x1c}}}{[k_0(-n_y^i + n_y')][k_0(-n_y^i + n_y'')]}\right.$$
$$\times\cos\left\{k_0\left[x_{d1}\left(-n_x^i + \frac{n_x{}' + n_x{}''}{2}\right) + h_{x1c}\frac{2B_1}{\langle h_x{}^2\rangle}\left(-n_y^i + \frac{n_y{}' + n_y{}''}{2}\right)\right]\right\}$$
$$\times\exp\left\{-k_0{}^2(-n_y^i + n_y')(-n_y^i + n_y'')\left[\langle h^2\rangle(1 - R_1) - \frac{2B_1{}^2}{\langle h_x{}^2\rangle}\right]\right\}$$
$$\times\exp\left[-\frac{1}{2}k_0{}^2\left(\langle h^2\rangle - \frac{B_1{}^2}{\langle h_x{}^2\rangle}\right)(n_y{}' - n_y{}'')^2\right]p(h_{x1c})\mathrm{d}h_{x1c}\mathrm{d}x_{d1}\left.\right)\left(2\int_{x_{d2}=0}^{\infty}\int_{h_{x2c}=-\infty}^{\infty}\frac{[D(\hat{n}^f, \hat{n}')D^*(\hat{n}^f, \hat{n}'')]_{h_{x2}{}'=h_{x2}{}''=h_{x2c}}}{[k_0(n_y^f - n_y')][k_0(n_y^f - n_y'')]}\right.$$
$$\times\cos\left\{k_0\left[x_{d2}\left(n_x^f - \frac{n_x{}' + n_x{}''}{2}\right) + h_{x2c}\frac{2B_2}{\langle h_x{}^2\rangle}\left(n_y^f - \frac{n_y{}' + n_y{}''}{2}\right)\right]\right\}$$
$$\times\exp\left\{-k_0{}^2(n_y^f - n_y')(n_y^f - n_y'')\left[\langle h^2\rangle(1 - R_1) - \frac{2B_2{}^2}{\langle h_x{}^2\rangle}\right]\right\}$$
$$\times\exp\left[-\frac{1}{2}k_0{}^2\left(\langle h^2\rangle - \frac{B_2{}^2}{\langle h_x{}^2\rangle}\right)(n_y{}' - n_y{}'')^2\right]p(h_{x2c})\mathrm{d}h_{x2c}\mathrm{d}x_{d2}\left.\right)$$
$$\times[1 - P_2(|n_y'|)][1 - P_2(|n_y''|)]\exp[jk_0(x_{c1} - x_{c2})(n_x{}' - n_x{}'')]\mathrm{d}x_{c1}\mathrm{d}x_{c2}\frac{\mathrm{d}n_y'}{[1 - (n_y')^2]^{1/2}}\frac{\mathrm{d}n_y''}{[1 - (n_y'')^2]^{1/2}}. \quad (26)$$

The variables x_{c1} and x_{c2} appear in Eq. (26) only as the difference $x_{c1} - x_{c2}$. Thus integral (26) can be expressed as

$$\langle \sigma_{pd} \rangle = \int_{n_y''=-1}^{1} \int_{n_y'=-1}^{1} \int_{x_{c1},x_{c2}=-L}^{L} f(n_y', n_y'') \times \exp[jk_0(x_{c1} - x_{c2})(n_x' - n_x'')] dx_{c1} dx_{2c} dn_y' dn_y''. \quad (27)$$

The integration variables in Eq. (27) are changed from x_{c1} and x_{c2} to x_m and x_c as follows:

$$x_m = x_{c1} - x_{c2}, \qquad x_c = \frac{x_{c1} + x_{c2}}{2}. \quad (28)$$

The region of integration for x_m and x_c is diamond shaped with end points at $\pm 2L$ and $\pm L$, respectively. However, since x_m is the distance between the midpoints of $1'$ and $1''$ and of $2'$ and $2''$, the limits of integration of this variable are assumed to be $(-L_m, L_m)$, where L_m is the width of a typical depression (or valley) on the rough surface (see Appendix C and Refs. 22 and 31). The fields that penetrate the rough surface are assumed to be absorbed in the conducting media. On assuming that $L_m \ll L$, the limits of integration are $-L_m < x_m < L_m$ and $-L < x_c < L$.

Equation (27) is integrated with respect to x_c and x_m, where we take into account that $n_x' = \pm[1 - (n_y')^2]^{1/2}$ for $x_m < 0$ and $x_m > 0$, respectively. Thus the total contributions to the cross sections from the quasi-parallel paths are

$$\langle \sigma_{pd} \rangle = 2(2L_m)(2L) \times \left\{ \int_{n_y'=-1}^{1} \int_{n_y''=n_y'}^{1} f_r \operatorname{sinc}[k_0 L_m (n_x' - n_x'')] dn_y'' dn_y' + \int_{n_y'=-1}^{1} \int_{n_y''=n_y'}^{1} f_i \sin\left[\frac{k_0 L_m}{2}(n_x' - n_x'')\right] \times \operatorname{sinc}\left[\frac{k_0 L_m}{2}(n_x' - n_x'')\right] dn_y'' dn_y' \right\}, \quad (29a)$$

where

$$f_r = \operatorname{Re}(f), \qquad f_i = \operatorname{Im}(f). \quad (29b)$$

Furthermore, in order to express Eq. (29a) in terms of real functions, we made use of the relationship $f(n_y', n_y'') = f^*(n_y'', n_y')$. Thus the limits of integration in Eq. (29a) are changed to $-1 \le n_y' \le 1$ and $n_y' \le n_y'' \le 1$ [half the corresponding range in Eq. (27)]. In the integrand of Eq. (29a) f_r and f_i are evaluated for $n_x' = [1 - (n_y')^2]^{1/2}$, $n_x'' = [1 - (n_y'')^2]^{1/2}$ and for $n_x' = -[1 - (n_y')^2]^{1/2}$, $n_x'' = -[1 - (n_y'')^2]^{1/2}$ (quasi-parallel case). The sum accounts for the cases $x_m < 0$ and $x_m > 0$. Most of the contributions to the integrand in Eq. (29a) come from the region where $\hat{n}' \approx \hat{n}''$.[11-13] Thus, in general, the second term in Eq. (29a) is negligibly small compared with the first term, since its integrand vanishes as $n_x' \to n_x''$. For perfectly conducting surfaces $f_i = 0$ holds, and in this case the second term is identically equal to zero.

When one uses standard techniques to evaluate the six-dimensional integrals (29) (over the variables h_{xc1}, h_{xc2}, x_{d1}, x_{d2}, n_y', and n_y'' [Eq. (26)], the required CPU time is excessive, even for supercomputers. To overcome this problem, we introduce the following substitutions for the wave-vector variables $\hat{n}'$ and $\hat{n}''$ in Eq. (29) (Ref. 25) (on making the assumption that the major contributions to the cross section come from the region $n_y' \approx n_y''$ for the quasi-parallel case):

$$\hat{n}_a = \frac{\hat{n}' + \hat{n}''}{2}, \qquad n_d = \hat{n}' - \hat{n}''. \quad (30)$$

Thus the expression for the quasi-parallel double-scatter cross section can be simplified to

$$\langle \sigma_{pd} \rangle = \frac{k_0^7}{2\pi^2}(2L_m) P_2(\hat{n}^i) P_2(\hat{n}^f) \times \int_{n_{dy}} \int_{n_{ay}} \langle \sigma_{pd1}(n_y', n_y'') \rangle \langle \sigma_{pd2}(n_y', n_y'') \rangle \times [1 - P_2(|n_y'|)][1 - P_2(|n_y''|)] \operatorname{sinc}[k_0 L_m (n_x' - n_x'')] \times \frac{dn_{ay}}{[1 - n_y')^2]^{1/2}} \frac{dn_{dy}}{[1 - n_y'')^2]^{1/2}}. \quad (31a)$$

The region of integration is half the diamond-shaped area with end points on the n_{ay} axis at $(-1, 1)$ and on the n_{dy} axis at $(-2, 2)$. The quantities $\langle \sigma_{pd1}(n_y', n_y'') \rangle$ and $\langle \sigma_{pd2}(n_y', n_y'') \rangle$ are associated with the single-scatter cross sections:

$$\langle \sigma_{pd1}(n_y', n_y'') \rangle = 2 \int_{x_{d1}=0}^{\infty} \int_{h_{x1c}=-\infty}^{\infty} \frac{\operatorname{Re}[D(\hat{n}', \hat{n}^i) D^*(\hat{n}'', \hat{n}^i)]}{[k_0(-n_y^i + n_y')][k_0(-n_y^i + n_y'')]} \times \cos\left\{ k_0 \left[x_{d1}\left(-n_x^i + \frac{n_x' + n_x''}{2}\right) + h_{x1c}\frac{2B_1}{\langle h_x^2 \rangle}\left(-n_y^i + \frac{n_y' + n_y''}{2}\right)\right]\right\} \times \exp\left\{ -k_0^2(-n_y^i + n_y')(-n_y^i + n_y'') \times \left[\langle h^2 \rangle (1 - R_1) - \frac{2B_1^2}{\langle h_x^2 \rangle}\right]\right\} \times \exp\left[-\frac{1}{2} k_0^2 \left(\langle h^2 \rangle - \frac{B_1^2}{\langle h_x^2 \rangle}\right)(n_y' - n_y'')^2\right] \times p(h_{x1c}) dh_{x1c} dx_{d1}, \quad (31b)$$

$$\langle \sigma_{pd2}(n_y', n_y'') \rangle = 2 \int_{x_{d2}=0}^{\infty} \int_{h_{x2c}=-\infty}^{\infty} \frac{\operatorname{Re}[D(\hat{n}^f, \hat{n}') D^*(\hat{n}^f, \hat{n}'')]}{[k_0(n_y^f + n_y')][k_0(n_y^f + n_y'')]} \times \cos\left\{ k_0 \left[x_{d2}\left(n_x^f - \frac{n_x' + n_x''}{2}\right) + h_{x2c}\frac{2B_2}{\langle h_x^2 \rangle}\left(n_y^f - \frac{n_y' + n_y''}{2}\right)\right]\right\} \times \exp\left\{ -k_0^2(n_y^f - n_y')(n_y^f - n_y'') \times \left[\langle h^2 \rangle (1 - R_2) - \frac{2B_2^2}{\langle h_x^2 \rangle}\right]\right\} \times \exp\left[-\frac{1}{2} k_0^2 \left(\langle h^2 \rangle - \frac{B_2^2}{\langle h_x^2 \rangle}\right)(n_y' - n_y'')^2\right] \times p(h_{x2c}) dh_{x2c} dx_{d2}. \quad (31c)$$

Note that the integrands of Eqs. (31b) and (31c) are real and that the limits on x_{dn} ($n = 1, 2$) are $(0, \infty)$. Thus Eqs. (31b) and (31c) can be evaluated as functions of n_{ay} with $n_{dy} = 0$ for the quasi-parallel case. The coherent scattered cross sections associated with $\langle\sigma_{pcn}\rangle$ are obtained from Eqs. (31b) and (31c) if we set $R_n = 0$ in Eq. (20). The incoherent scatter cross section is defined as

$$\langle\sigma_{pIn}\rangle = \langle\sigma_{pdn}\rangle - \langle\sigma_{pcn}\rangle. \tag{32}$$

In Eqs. (31) the integrand of the quasi-parallel double-scatter cross section is expressed in terms of a product of two integrals, σ_{pdn} ($n = 1, 2$), associated with single-scatter cross sections. In the high-frequency (stationary phase) limit they can be evaluated in closed form.[11–13] Since the full-wave solutions account for upward and downward scattered waves, the quantities $-n_y^i + n_y'$, $-n_y^i + n_y''$, $n_y^f - n_y'$, and $n_y^f - n_y''$ could be positive or negative. The interaction between these two single-scatter cross sections is accounted for by the function $\mathrm{sinc}[k_0 L_m(n_x' - n_x'')]$. The major contributions to the integrands in Eqs. (31) come from the regions where $\hat{n}' \approx \hat{n}''$ {on account of the terms $\exp[-k_0^2\langle h^2\rangle(n_y' - n_y'')^2]$ and $\mathrm{sinc}[k_0 L_m(n_x' - n_x'')]$ that appear in the integrand}. Thus Eqs. (31) are referred to as the quasi-parallel ($\hat{n}' \approx \hat{n}''$) contribution to the double-scatter cross section.

For the quasi-antiparallel ($\hat{n}' \approx -\hat{n}''$) path [see Fig. 2(b)] the surface variables are grouped into the two pairs of points x_{s1}', x_{s2}'', and x_{s2}', x_{s1}''. In this case the following changes in the variables of integration are made instead of Eqs. (11):

$$x_{d1} = x_{s1}' - x_{s2}'', \qquad x_{d2} = x_{s2}' - x_{s1}'', \tag{33a}$$

$$x_{c1} = \frac{x_{s1}' + x_{s2}''}{2}, \qquad x_{c2} = \frac{x_{s2}' + x_{s1}''}{2}. \tag{33b}$$

For the quasi-antiparallel case it is assumed that the slopes at x_{s1}' and x_{s2}'' (h_{x1}' and h_{x2}'', respectively) on the rough surface are approximately equal to the slope h_{x1c} at the midpoint x_{c1}. Similarly, the slopes at the points x_{s2}' and x_{s1}'' (h_{x2}' and h_{x1}'', respectively) on the rough surface are equal to the slope h_{x2c} at the midpoint x_{c2}.[28] The correlations between the heights at x_{s1}' and x_{s2}'' and the slope at x_{1c} are given by $\pm B_1$, and those between the heights at x_{s2}' and x_{s1}'' and the slope at x_{2c} are given by $\pm B_2$. The surface height autocorrelation functions at these pairs of points are given by R_1 and R_2, respectively. Thus, in this case, X_{np} in Eq. (18) is replaced by

$$X_{na} = \begin{pmatrix} h_n' \\ h_m'' \\ h_{xnc} \end{pmatrix}, \quad n, m = 1, 2; \quad n \neq m. \tag{34}$$

The above substitutions for the surface variables in Eq. (10) can be shown to yield the following expressions for the double-scatter quasi-antiparallel cross sections:

$$\begin{aligned}\langle\sigma_{ad}\rangle = {} & \frac{k_0^7}{2\pi^2}(2Lm)P(\hat{n}^i)P(\hat{n}^f) \\ & \times \int_{n_{ay}} \int_{n_{dy}} \langle\sigma_{ad1}(n_y', n_y'')\rangle\langle\sigma_{ad2}(n_y', n_y'')\rangle \\ & \times [1 - P_2(|n_y'|)][1 - P_2(|n_y''|)] \\ & \times \mathrm{sinc}[k_0 L_m(n_x^f + n_x^i - n_x' - n_x'')] \\ & \times \frac{\mathrm{d}n_{dy}}{[1 - (n_y')^2]^{1/2}} \frac{\mathrm{d}n_{ay}}{[1 - (n_y'')^2]^{1/2}}.\end{aligned} \tag{35a}$$

The region of the integration is half the diamond-shaped area with end points on the n_{ay} axis at $(-1, 1)$ and on the n_{dy} axis at $(-2, 2)$. The quantities $\langle\sigma_{ad1}(n_y', n_2'')\rangle$ and $\langle\sigma_{ad2}(n_y', n_2'')\rangle$ are associated with the single-scatter cross sections:

$$\begin{aligned}&\langle\sigma_{ad1}(n_y', n_y'')\rangle \\ &= 2\int_{x_{d1}=0}^{\infty} \int_{h_{x1c}=-\infty}^{\infty} \frac{\mathrm{Re}[D(\hat{n}', \hat{n}^i)D^*(\hat{n}^f, \hat{n}'')]}{[k_0(-n_y^i + n_y')][k_0(n_y^f + n_y'')]} \\ &\quad \times \cos\left\{k_0\left[\frac{x_{d1}}{2}(n_x^f - n_x^i + n_x' + n_x'') \right.\right. \\ &\quad \left.\left. + h_{x1c}\frac{B_1}{\langle h_x^2\rangle}(n_y^f - n_y^i + n_y' - n_y'')\right]\right\} \\ &\quad \times \exp\left\{-k_0^2(-n_y^i + n_y')(-n_y^i + n_y'') \right. \\ &\quad \left. \times [\langle h^2\rangle(1 - R_1) - \frac{2B_1^2}{\langle h_x^2\rangle}]\right\} \\ &\quad \times \exp\left[-\frac{1}{2}k_0^2\left(\langle h^2\rangle - \frac{B_1^2}{\langle h_x^2\rangle}\right)\right. \\ &\quad \left. \times (-n_y^i + n_y' - n_y^f + n_y'')^2\right] p(h_{x1c})\mathrm{d}h_{x1c}\mathrm{d}x_{d1},\end{aligned} \tag{35b}$$

$$\begin{aligned}&\langle\sigma_{ad2}(n_y', n_y'')\rangle \\ &= 2\int_{x_{d2}=0}^{\infty} \int_{h_{x2c}=-\infty}^{\infty} \frac{\mathrm{Re}[D(\hat{n}^f, \hat{n}')D^*(\hat{n}'', \hat{n}^i)]}{[k_0(n_y^f - n_y')][k_0(-n_y^i + n_y'')]} \\ &\quad \times \cos\left\{k_0\left[\frac{x_{d2}}{2}(n_x^f - n_x^i + n_x' - n_x'') \right.\right. \\ &\quad \left.\left. + h_{x2c}\frac{B_2}{\langle h_x^2\rangle}(n_y^f - n_y^i + n_y' - n_y'')\right]\right\} \\ &\quad \times \exp\left\{-k_0^2(-n_y^i + n_y')(-n_y^i + n_y'') \right. \\ &\quad \left. \times \left[\langle h^2\rangle(1 - R_2) - \frac{2B_2^2}{\langle h_x^2\rangle}\right]\right\} \\ &\quad \times \exp\left[-\frac{1}{2}k_0^2\left(\langle h^2\rangle - \frac{B_2^2}{\langle h_x^2\rangle}\right)\right. \\ &\quad \left. \times (-n_y^i + n_y' - n_y^f + n_y'')^2\right] p(h_{x2c})\mathrm{d}h_{x2c}\mathrm{d}x_{d2}.\end{aligned} \tag{35c}$$

The coherent scatter cross sections associated with $\langle\sigma_{acn}\rangle$ can be obtained from Eqs. (35b) and (35c) if we set $R_n = 0$. The incoherent scatter cross section is

$$\langle\sigma_{aIn}\rangle = \langle\sigma_{adn}\rangle - \langle\sigma_{acn}\rangle. \tag{36}$$

Thus, as for the quasi-parallel case, the integrand of the diffuse double-scatter quasi-antiparallel cross section is expressed as a product of two terms, $\langle\sigma_{adn}\rangle$ ($n = 1, 2$), associated with single-scatter cross sections. The interaction between these two single-scatter cross sections is accounted for by the function $\mathrm{sinc}[k_0 L_m(n_x^f + n_x^i - n_x' - n_x'')]$. The major contributions to the observed sharp backscatter intensity come from the regions where the arguments of the terms $\exp[-k_0^2\langle h^2\rangle(-n_y^i n_y'' - n_y^f + n_y')^2]$ and $\mathrm{sinc}[k_0 L_m(n_x^f + n_x^i - n_x' - n_x'')]$ are very small. In

view of the presence of the shadow functions $[1 - P_2(|n_y'|)]$ $[1 - P_2(|n_y''|)]$, this occurs for the antiparallel case ($\hat{n}' \approx \hat{n}''$) in the backscatter direction ($\hat{n}^f = -\hat{n}^i$). Thus the quasi-antiparallel double-scatter cross section accounts for the observed backscatter enhancement.

As for the quasi-parallel case [Eqs. (31)], to evaluate Eqs. (35) it is necessary only to evaluate real integrals. This speeds up the numerical evaluation of the integrals significantly and also increases the accuracy of the results. The integrands (35) are evaluated for $n_x' = [1 - (n_y')^2]^{1/2}$, $n_x'' = -[1 - (n_y'')^2]^{1/2}$ and for $n_x' = [1 - (n_y')^2]^{1/2}$, $n_x'' = [1 - (n_y'')^2]^{1/2}$ (quasi-antiparallel case) and are summed.

In Eq. (31) the two-dimensional integrals for $\langle \sigma_{pIn} \rangle$ ($n = 1, 2$) with respect to h_{xnc} and x_{dn} are evaluated independently as functions of n_{ay} only, since $\hat{n}' \approx \hat{n}'' \approx \hat{n}_a$ for the quasi-parallel case. Similarly, in Eqs. (35) the two-dimensional integrals for $\langle \sigma_{aIn} \rangle$ ($n = 1, 2$) are evaluated as functions of n_{dy} only, since $\hat{n}' \approx \hat{n}'' \approx \hat{n}_d/2$ for the quasi-antiparallel case. Thus the six-dimensional integrals are, for practical purposes, computed as three-dimensional integrals.

3. ILLUSTRATIVE EXAMPLES

The full-wave diffuse single-scatter and diffuse double-scatter cross sections $\langle \sigma \rangle$ (quasi-parallel and quasi-antiparallel) are plotted in Figs. 3–14 as functions of $\theta^f \cos \phi^f$ (where $\phi^i - \phi^f = 0, \pi$) for the vertically and horizontally polarized waves. In Figs. 3–8 the corresponding experimental results are also plotted.[5] The incident angles are $\theta^i = 0°$, 10°, and 30°. The one-dimensional rough surface considered in the examples is characterized by a Gaussian surface height autocorrelation function [Eq. (20)]. Its root-mean-square height is $(\langle h^2 \rangle) = 1.73$ μm, and its correlation length is $l_c = 3.43$ μm. Experimental (scatter cross sections and Mueller matrix elements) data have been published recently for this surface.[5] The data presented here are renormalized such that the total power W scattered above the rough interface, per unit of incident power, is

$$W = \int_0^{\pi/2} \langle \sigma_N \rangle_{\phi=0} \, d\theta + \int_0^{\pi/2} \langle \sigma_N \rangle_{\phi=\pi} \, d\theta, \qquad (37a)$$

and thus

$$\langle \sigma_N \rangle = \frac{\langle \sigma \rangle}{2\pi \cos \theta_0{}^i}. \qquad (37b)$$

In Figs. 3–8 the free-space wavelength is $\lambda = 1.152$ μm, and in Figs. 9–14 the wavelength is $\lambda = 3.392$ μm. The relative complex permittivity of gold is assumed to be $\epsilon_r = -62.787 - j4.948$ at $\lambda = 1.152$ μm and $\epsilon_r = -424.64 - j81.144$ at $\lambda = 3.392$ μm. The Rayleigh roughness parameter $\beta = 4k_0{}^2\langle h^2 \rangle = 356.128$ at $\lambda = 1.152$ μm and $\beta = 41.077$ at $\lambda = 3.392$ μm. The mean-square slope of the (Gaussian) rough surface is $\langle h_x{}^2 \rangle = 2\langle h^2 \rangle / (l_c)^2 = 0.508$. For all the examples the double-scatter mean distance is assumed to be $L_m = 11.13 l_c$ (Ref. 22) (see Appendix C).

The sharp enhancement in the cross section $\langle \sigma \rangle$ is observed for both the vertical and horizontal polarizations at backscatter, where $\theta^i = \theta^f$ and $\phi^i - \phi^f = \pi$. In Figs. 3, 6, 9, and 12 $\theta^i = 0°$, in Figs. 4, 7, 10, and 13 $\theta^i = 10°$, and in Figs. 5, 8, 11, and 14 $\theta^i = 30°$. The enhanced backscatter is due to contributions of the quasi-antiparallel paths ($\hat{n}' \approx -\hat{n}''$) to the double-scatter cross sections [see Fig. 2(b)].[22–24] To emphasize this important result, we have plotted both the quasi-parallel ($\hat{n}' \approx \hat{n}''$) and quasi-antiparallel ($\hat{n}' \approx -\hat{n}''$) double-scatter contributions to the cross sections as functions of $\theta^f \cos \phi^f$ in Fig. 15 for the vertically polarized case. In this figure the incident angle is $\theta^i = 10°$, and the wavelength used is $\lambda = 1.152$ μm.

In order to examine the polarization dependence of the diffuse double-scatter cross sections (quasi-parallel and quasi-antiparallel), we plot the vertically and horizontally

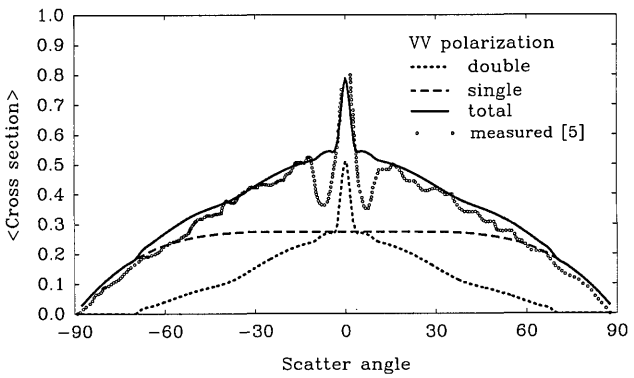

Fig. 3. Vertically polarized single-, double-, and total- (single + double) scatter average cross sections plotted versus scatter angle (scatter angle $\equiv \theta^f \cos \phi^f$ for $\phi^f = 0, \pi$ and $\phi^i = 0$) for $\theta^i = 0°$, $\beta = 356.128$, $\langle h_x{}^2 \rangle = 0.508$, $\lambda = 1.152$ μm, and $\epsilon_r = -62.787 - j4.948$.

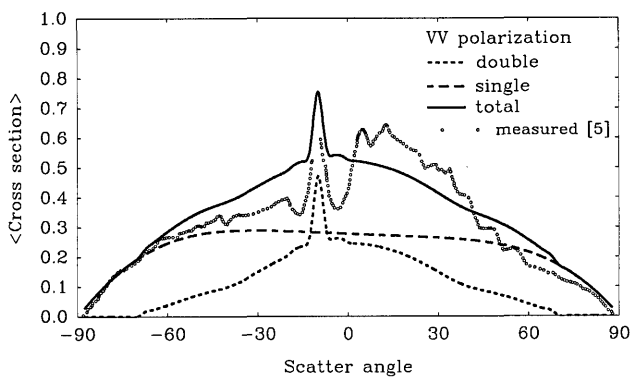

Fig. 4. Same as Fig. 3 but for $\theta^i = 10°$.

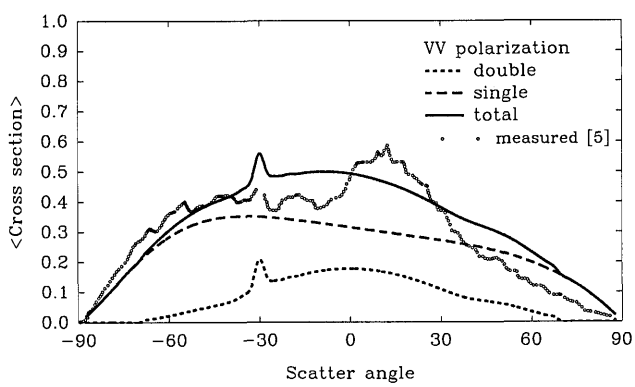

Fig. 5. Same as Fig. 3 but for $\theta^i = 30°$.

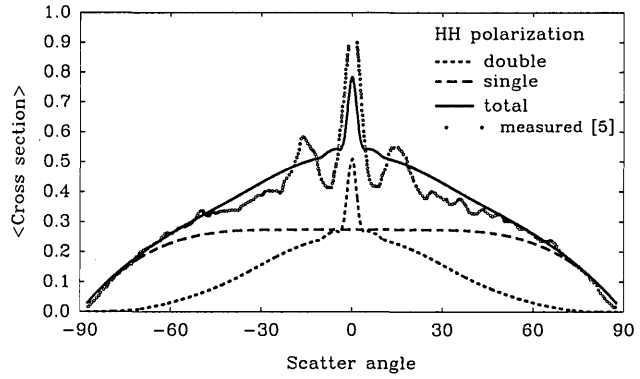

Fig. 6. Horizontally polarized single-, double-, and total- (single + double) scatter average cross sections plotted versus scatter angle (scatter angle $\equiv \theta^f \cos\phi^f$ for $\phi^f = 0, \pi$ and $\phi^i = 0$) for $\theta^i = 0°$, $\beta = 356.128$, $\langle h_x{}^2\rangle = 0.508$, $\lambda = 1.152$ μm, and $\epsilon_r = -62.787 - j4.948$.

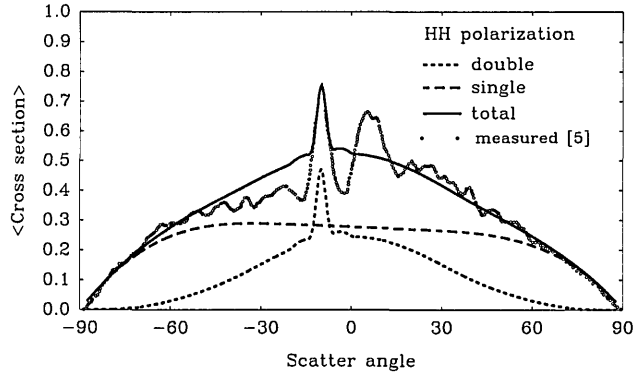

Fig. 7. Same as Fig. 6 but for $\theta^i = 10°$.

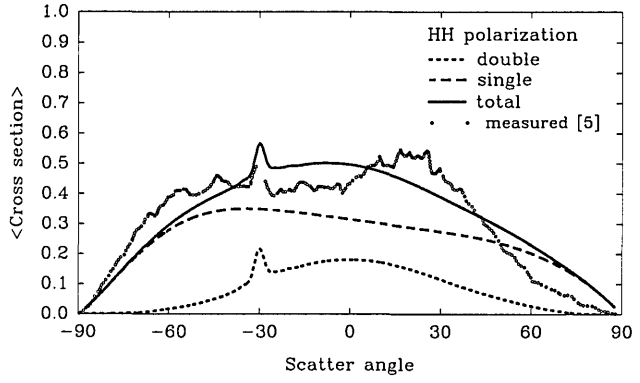

Fig. 8. Same as Fig. 6 but for $\theta^i = 30°$.

polarized results in Figs. 16 and 17 for $\lambda = 1.152$ μm and $\lambda = 3.392$ μm, respectively. At the higher frequency (Fig. 16, $\lambda = 1.152$ μm) both the single- and double-scatter cross sections for the vertical and horizontal polarizations tend to merge. At the higher frequency the significant contributions to the scattered cross sections come from the neighborhood of the stationary-phase (specular) points. At the stationary-phase points the surface element scattering coefficients (13) are proportional to the Fresnel reflection coefficients.[32] Since the surface of gold is highly reflective, the magnitude of the Fresnel reflection coefficients is approximately equal to unity for both vertical and horizontal polarizations. At the lower frequency (Fig. 17, $\lambda = 3.392$ μm) significant polarization dependence is observed for the double-scatter cross sections (including the backscatter direction). When high-frequency (stationary-phase) approximations are used to obtain the double-scatter cross sections,[11–13] the approximate results are practically independent of the polarization even at the lower frequency. The stationary-phase (specular point) results cannot be used when the polarization dependence is a significant factor.

The results given in Figs. 3–14 show that the angular width of the sharp enhanced backscatter also depends on frequency. The enhanced backscatter angular width is larger at the lower frequency (the Rayleigh parameter is $\beta = 41.077$) than at the higher frequency ($\beta = 356.128$).

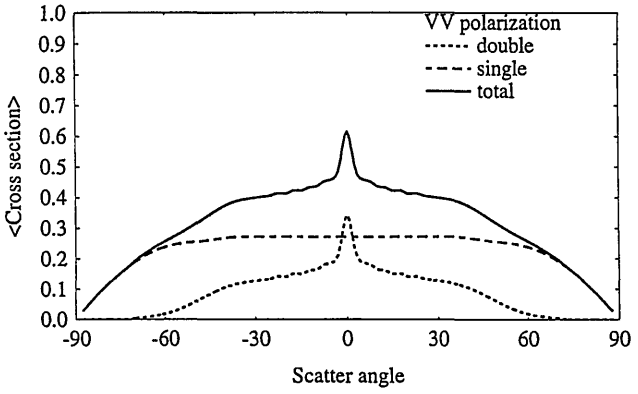

Fig. 9. Vertically polarized single-, double-, and total- (single + double) scatter average cross sections plotted versus scatter angle (scatter angle $\equiv \theta^f \cos\phi^f$ for $\phi^f = 0, \pi$ and $\phi^i = 0$) for $\theta^i = 0°$, $\beta = 41.077$, $\langle h_x{}^2\rangle = 0.508$, $\lambda = 3.392$ μm, and $\epsilon_r = -424.648 - j81.144$.

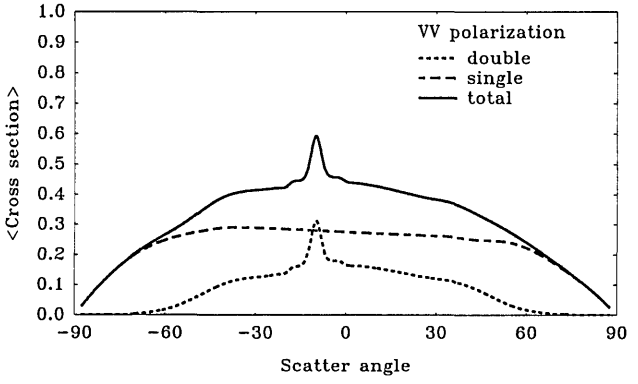

Fig. 10. Same as Fig. 9 but for $\theta^i = 10°$.

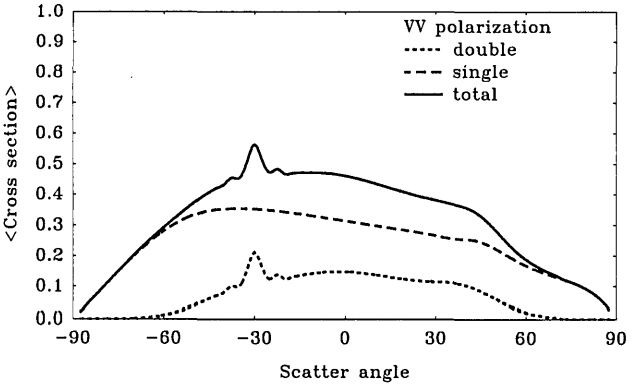

Fig. 11. Same as Fig. 9 but for $\theta^i = 30°$.

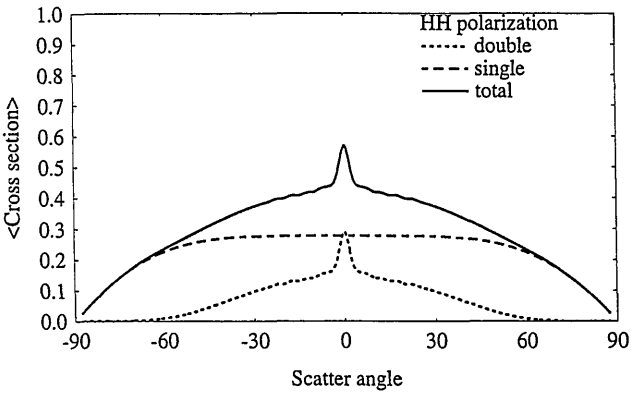

Fig. 12. Horizontally polarized single-, double-, and total-(single + double) scatter average cross sections plotted versus scatter angle (scatter angle $\equiv \theta^f \cos\phi^f$ for $\phi^f = 0, \pi$ and $\phi^i = 0$) for $\theta^i = 0°$, $\beta = 41.077$, $\langle h_x{}^2\rangle = 0.508$, $\lambda = 3.392$ μm, and $\epsilon_r = -424.648 - j81.144$.

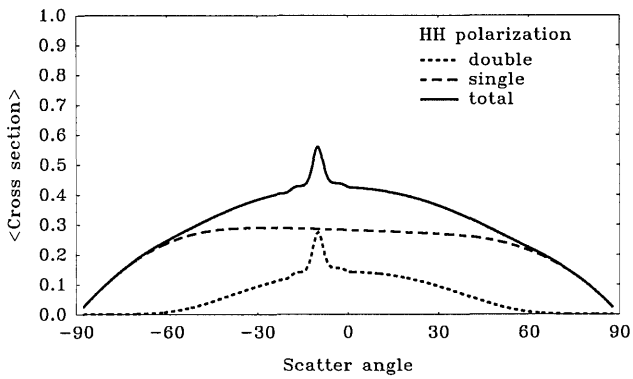

Fig. 13. Same as Fig. 12 but for $\theta^i = 10°$.

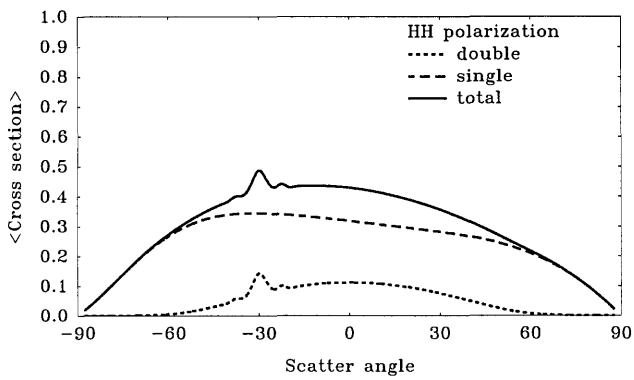

Fig. 14. Same as Fig. 12 but for $\theta^i = 30°$.

When the high-frequency stationary-phase approximations are used,[11–13,22] the angular width of the sharply enhanced backscatter is significantly smaller, especially for the higher frequency ($\beta = 356.128$).

The effects of varying the mean-square height on the enhanced backscatter peak are illustrated by the plots in Fig. 18. The Rayleigh roughness parameters considered in these plots are in the range $3 \le \beta \le 300$. The level of the peak does not increase significantly for values of β larger than 300. However, for $\beta \le 3$ there is practically no enhanced backscatter. The mean-square-height-dependent factor that has the major effect on the level of the backscatter peak is $\exp[-\frac{1}{2}k_0{}^2\langle h^2\rangle(n_y{}^i + n_y{}^f - n_y{}' - n_y{}'')]$. It appears in the expression for the conditional joint characteristic function χ_{2n} [Eq. (24)]. Thus, as $k_0{}^2\langle h^2\rangle$ increases, the angular width of the peak about the backscatter direction ($\hat{n}^f = -\hat{n}^i$) decreases.

The effects of varying the mean-square slope on the enhanced backscatter peak are illustrated by the plots in Fig. 19. The mean-square slopes considered here are $\langle h_x{}^2\rangle = 0.508, 1, 1.5, 2$. The mean-square-

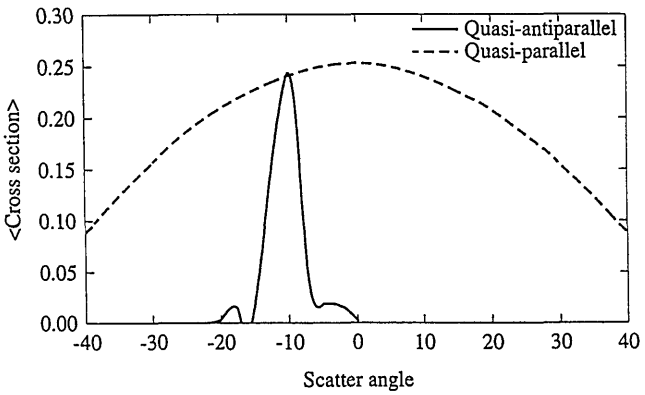

Fig. 15. Vertically polarized double quasi-parallel and quasi-antiparallel scatter average cross sections plotted versus scatter angle (scatter angle $\equiv \theta^f \cos\phi^f$ for $\phi^f = 0, \pi$ and $\phi^i = 0$) for $\theta^i = 10°$, $\beta = 356.128$, $\langle h_x{}^2\rangle = 0.508$, $\lambda = 1.152$ μm, and $\epsilon_r = -62.787 - j4.948$.

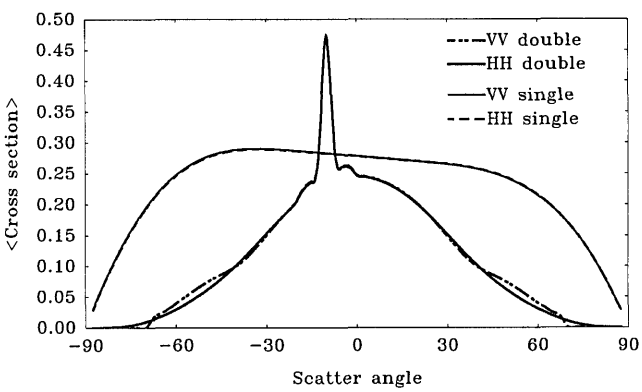

Fig. 16. Vertically and horizontally polarized single- and double-scatter average cross sections plotted versus scatter angle (scatter angle $\equiv \theta^f \cos\phi^f$ for $\phi^f = 0, \pi$ and $\phi^i = 0$) for $\theta^i = 10°$, $\beta = 356.128$, $\langle h_x{}^2\rangle = 0.508$, $\lambda = 1.152$ μm, and $\epsilon_r = -62.787 - j4.948$.

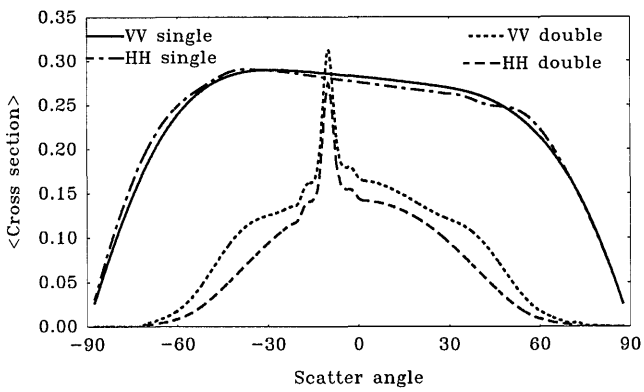

Fig. 17. Same as Fig. 16 but for $\theta^i = 10°$, $\beta = 41.077$, $\langle h_x{}^2\rangle = 0.508$, $\lambda = 3.392$ μm, and $\epsilon_r = -424.648 - j81.144$.

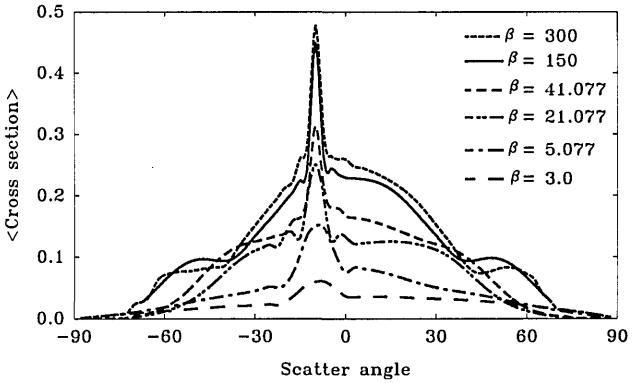

Fig. 18. Vertically polarized double-scatter average cross sections plotted versus scatter angle (scatter angle $\equiv \theta^f \cos \phi^f$ for $\phi^f = 0$, π and $\phi^i = 0$) for different values of β and for $\theta^i = 10°$, $\langle h_x{}^2 \rangle = 0.508$, $\lambda = 3.392$ μm, and $\epsilon_r = -424.648 - j81.144$.

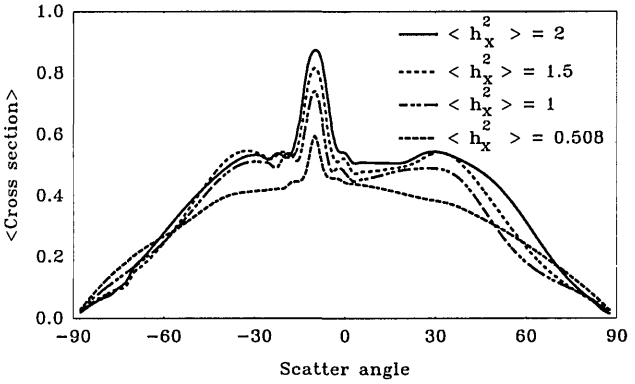

Fig. 19. Vertically polarized total- (single + double) scatter average cross sections plotted versus scatter angle (scatter angle $\equiv \theta^f \cos \phi^f$ for $\phi^f = 0$, π and $\phi^i = 0$) for different values of mean-square slope $\langle h_x{}^2 \rangle$ and for $\theta^i = 10°$, $\beta = 41.077$, $\lambda = 3.392$ μm, and $\epsilon_r = -424.648 - j81.144$.

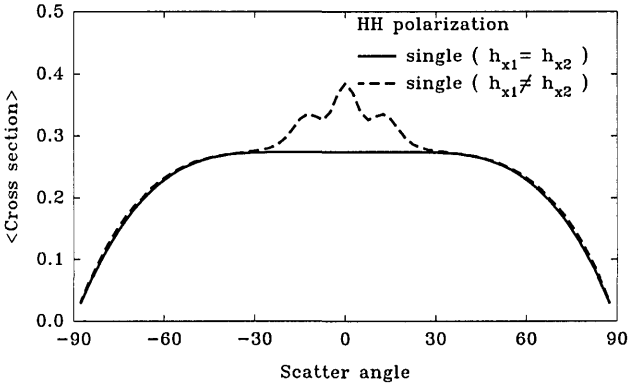

Fig. 20. Horizontally polarized single-scatter average cross sections plotted versus scatter angle (scatter angle $\equiv \theta^f \cos \phi^f$ for $\phi^f = 0$, π and $\phi^i = 0$) for $\theta^i = 0°$, $\beta = 356.128$, $\langle h_x{}^2 \rangle = 0.508$, $\lambda = 1.152$ μm, and $\epsilon_r = -62.787 - j4.948$, where $h_{x1} = h_{x2}$ means that the large radius of curvature assumption is used and $h_{x1} \neq h_{x2}$ means that it is not used.

slope-dependent factor that has a major effect on the level of the backscatter peak is $\exp(\frac{1}{2}\langle h_x{}^2 \rangle k_0{}^2 \{(x_{dn}/2) \exp[-(x_{dn}/2l_c)^2]\}^2 (n_y{}^i + n_y{}^f - n_y{}' - n_y{}'')^2)$. It also appears in the expression for the conditional joint characteristic function χ_{2n} [Eq. (24)]. The level of the peak increases as the mean-square slope increases, and broad secondary peaks appear on both sides of the enhanced backscatter peak. However, for $\langle h_x{}^2 \rangle \geq 2$ the level of the enhanced backscatter peak does not increase appreciably.

For all the results plotted in Figs. 3–19 the analysis is based on the assumption that the radii of curvature are large compared with wavelength [Eq. (13)]. In Figs. 20–23 the effect of this simplifying assumption is examined. When the large radii of curvature assumption is not made (to compute the single-scatter cross sections), it is necessary to consider a four-variable joint probability-density function, $p(h_1, h_2, h_{x1}, h_{x2})$,[10] rather than the three-variable joint probability-density

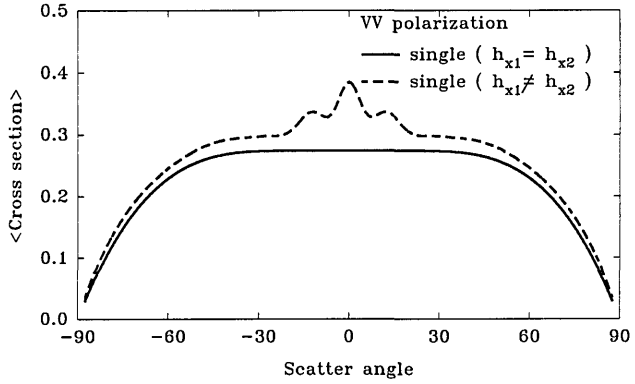

Fig. 21. Vertically polarized single-scatter average cross sections plotted versus scatter angle (scatter angle $\equiv \theta^f \cos \phi^f$ for $\phi^f = 0$, π and $\phi^i = 0$) for $\theta^i = 0°$, $\beta = 356.128$, $\langle h_x{}^2 \rangle = 0.508$, $\lambda = 1.152$ μm, and $\epsilon_r = -62.787 - j4.948$, where $h_{x1} = h_{x2}$ means that the large radius of curvature assumption is used and $h_{x1} \neq h_{x2}$ means that it is not used.

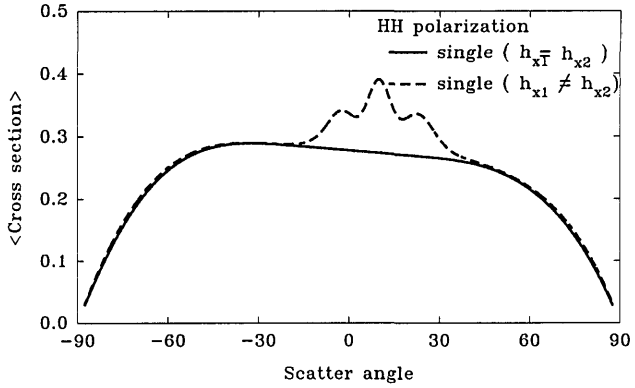

Fig. 22. Same as Fig. 20 but for $\theta^i = 10°$.

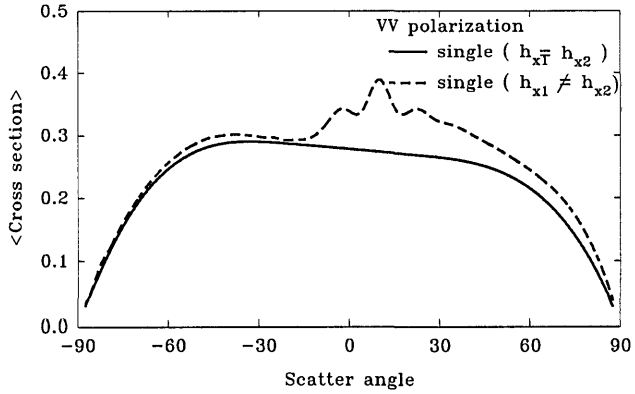

Fig. 23. Same as Fig. 21 but for $\theta^i = 10°$.

function $p(h_1, h_2, h_{xc}) = p(h_1, h_2 \mid h_{xc})p(h_{xc})$.[17] They are associated with the conditional joint characteristic functions $\chi_2(a, b \mid h_{x1}, h_{x2})$ (Ref. 10) and $\chi_2(a, b \mid h_{xc})$,[25] respectively. Thus, for the results plotted in Figs. 20–23, the derivations of the single-scatter cross sections are similar to those given in the earlier analysis.[10] In these plots for $\theta^i = 0°$ (Figs. 20 and 21) we observe a double hump about the sharp peak in the specular/backscatter directions. Furthermore, for $\theta^i = 10°$ (Figs. 22 and 23) we observe that this double hump appears in the quasi-specular direction. These observations appear to be in agreement with published experimental results.[4,5] Thus the observations of the secondary quasi-specular peaks are related to the nonnegligible effects of the radii of curvature. These are associated with the small-scale roughness of the random rough surface.

4. CONCLUSIONS

In the current paper we have computed and added incoherently both the single diffuse and double diffuse scatter cross sections to obtain the total diffuse cross section.[22] Correlations between the heights and the slopes at pairs of points on the rough surface are considered. We used the full-wave approach to obtain multidimensional integral expressions for the single- and double-scatter diffuse cross sections. With the use of transformations of variables (associated with the quasi-parallel and quasi-antiparallel paths) the six-dimensional integrals are evaluated essentially as three-dimensional integrals. When the full-wave stationary-phase approximation is used,[11–13] two-dimensional integral expressions for the double-scatter cross sections are obtained from the six-dimensional integral. The high-frequency approximate results for the single-scatter cross sections are in good agreement with the results presented here. However, the high-frequency approximations for the double scatter are practically independent of polarization, and the angular width of the enhanced backscatter is relatively very small.

The full-wave expressions for the double-scatter cross sections [Eqs. (31a) and (35a)] contain expressions associated with two single-scatter cross sections [Eqs. (31b), (31c) and (35b), (35c)]. The major contributions to the double-scatter integrals come from the regions where $\hat{n}'$ and $\hat{n}''$ are practically horizontal (near grazing with respect to the mean plane).[11–13] The stationary-phase approximations used to evaluate the quantities in Eqs. (31b), (31c) and (35b), (35c) become less valid at grazing angles ($\hat{n}' \approx \pm\hat{n}'' \approx \pm\hat{a}_x$). Thus, while the high-frequency results are useful in providing physical insight into the multiple-scatter problem, they do not provide satisfactory results for the polarization dependence and for the angular width of the enhanced backscatter. The double-scatter cross sections are expressed in terms of a product of two single-scatter cross sections that can be computed in parallel. The sinc functions represent the interactions between these two single-scatter cross sections.

For these surfaces the sharp enhancement (approximately 10° angular width) about the backscatter direction is due to double scatter rather than to single scatter.[33] This is in agreement with the results of Mendez and O'Donnell[1,2] and the results of Ishimaru and Chen.[22] However, there are very significant differences between the full-wave approach (based on the solution for the double scatter from a deterministic surface depression) and the physical optics approach (see Appendix B). These differences have a major effect on the angular width of the enhanced backscatter and on the polarization dependence of the results.

The effects of the shadowing P_2, the mean double-scatter path L_m, the mean-square height $\langle h^2 \rangle$, and the mean-square slope $\langle h_x^2 \rangle$ on the double-scatter results are revealed in the analytical expressions for the full-wave quasi-parallel and quasi-antiparallel contributions to the cross sections. Thus the shadow function factors $[1 - P_2(|\hat{n}'|)][1 - P_2(|\hat{n}''|)]$ maximize the integrand when $\hat{n}'$ and $\hat{n}''$ are practically horizontal ($\hat{n}' \approx \pm\hat{n}'' \approx \pm\hat{a}_x$). The enhanced backscatter level is maximum when the double-scatter mean path L_m is approximately $22l_c$. However, the level of the backscatter peak is not critically dependent on L_m for $5l_c \le L_m \le 30l_c$ (see Appendix C and Fig. 24). The effects of varying the mean-square height and the mean-square slope are illustrated in Figs. 18 and 19.

Note that the expressions derived here for the incoherent (single and double) scatter cross sections per unit area (width) are independent of the area (width) for all incident angles. The effect of the large radii of curvature assumptions is also examined here.

APPENDIX A

The following changes are made in the equations that appear in the cited papers by Bahar and El-Shenawee[6–9]:

(1) The slope-dependent surface element scattering coefficients $D^P(\hat{n}^f, \hat{n}^i)$ are rewritten as[19]

$$D^P(\hat{n}^f, \hat{n}^i) = 2(\cos\theta_0^{fn})(\cos\theta_0^{in})R^P(\hat{n}^f, \hat{n}^i) \times S(\hat{n}^f \cdot \hat{n})S(-\hat{n}^i \cdot \hat{n}), \quad P = V \text{ or } H, \tag{A1}$$

with

$$R^V = \frac{[\mu_r C_1^{in} C_1^{fn} \cos(\phi^{fn} - \phi^{in}) - S_0^{in} S_0^{fn}](1 - 1/\epsilon_r) + (1 - \mu_r)\cos(\phi^{fn} - \phi^{in})}{(C_0^{in} + \eta_r C_1^{in})(C_0^{fn} + \eta_r C_1^{fn})}, \tag{A2}$$

$$R^H = \frac{[\epsilon_r C_1^{in} C_1^{fn} \cos(\phi^{fn} - \phi^{in}) - S_0^{in} S_0^{fn}](1 - 1/\mu_r) + (1 - \epsilon_r)\cos(\phi^{fn} - \phi^{in})}{(C_0^{in} + C_1^{in}/\eta_r)(C_0^{fn} + C_1^{fn}/\eta_r)}, \tag{A3}$$

where $S(-\hat{n}^i \cdot \hat{n})$ is the unit step function associated with self-shadow for the incident waves and $S(\hat{n}^f \cdot \hat{n})$ is the unit step function associated with self-shadow for the scattered waves.

(2) In Eq. (A1) the term $k_0(n_y' - n_y^i)$ is not included in the definition of the slope-dependent surface element scattering coefficient $D^P(\hat{n}^f, \hat{n}^i)$, since it was obtained on integration by parts. Thus the terms $k_0(n_y' - n_y^i)$ and

$k_0(n_y^f - n_y')$ are not transformed to the local coordinate system, as they were in earlier studies.[6-9]

(3) Since $\langle h \rangle$, the mean value of the surface height, is zero (the mean plane is horizontal), the factor $\hat{n} \cdot \hat{a}_y$ (where $\hat{n}$ is the unit vector normal to the rough surface) is not included in the denominator of Eq. (1).

For the small-slope case (the quantity in the denominator of the integrand) $(-\mathbf{k}_0^i + \mathbf{k}_0') \cdot \hat{n}(\hat{n} \cdot \hat{a}_y) \approx (-\mathbf{k}_0^i + \mathbf{k}_0') \cdot \hat{a}_y$ and $(\mathbf{k}_0^f - \mathbf{k}_0') \cdot \hat{n}(\hat{n} \cdot \hat{a}_y) \approx (\mathbf{k}_0^f - \mathbf{k}_0') \cdot \hat{a}_y$, and for the high-frequency case $(-\mathbf{k}_0^i + \mathbf{k}_0') \cdot \hat{n}_s(\hat{n}_s \cdot \hat{a}_y) \rightarrow (-\mathbf{k}_0^i + \mathbf{k}_0') \cdot \hat{a}_y$ and $(\mathbf{k}_0^f + \mathbf{k}_0') \cdot \hat{n}_s(\hat{n}_s \cdot \hat{a}_y) \rightarrow (\mathbf{k}_0^f - \mathbf{k}_0') \cdot \hat{a}_y$. Thus, in these limits, the earlier solutions give approximately the same results as the current solutions. However, when $(-\mathbf{k}_0^i + \mathbf{k}_0') \cdot \hat{a}_y \rightarrow 0$ or $(\mathbf{k}_0^f - \mathbf{k}_0') \cdot \hat{a}_y \rightarrow 0$, the changes could be significant.

If the mean plane of the rough surface is perpendicular to the unit vector $\hat{n}_0 = n_{0x}\hat{a}_x + n_{0y}\hat{a}_y$, the quantity [in the denominator of the integrand of Eq. (6b)] $k_0(-n_y^i + n_y') = (-\mathbf{k}_0^i + \mathbf{k}_0') \cdot \hat{a}_y$ is replaced by $(-\mathbf{k}_0^i + \mathbf{k}_0') \cdot \hat{n}_0$ and the quantity $k_0(n_y^f - n_y') = (\mathbf{k}_0^f - \mathbf{k}_0') \cdot \hat{a}_y$ is replaced by $(\mathbf{k}_0^f - \mathbf{k}_0') \cdot \hat{n}_0$. Furthermore, $dx_{s1}'dx_{s2}'$ should be replaced by $[dx_{s1}'/(\hat{n}_0 \cdot \hat{a}_y)][dx_{s2}'/(\hat{n}_0 \cdot \hat{a}_y)]$.

The integrand of Eq. (6b) remains finite as $(-\mathbf{k}_0^i + \mathbf{k}_0') \cdot \hat{a}_y = k_0(-n_y^i + n_y') \rightarrow 0$ and/or as $(\mathbf{k}_0^f - \mathbf{k}_0') \cdot \hat{a}_y = k_0(n_y^f - n_y') \rightarrow 0$, since in these cases $\exp[-jk_0h(x_{s1}')(n_y^i - n_y')] - 1 \rightarrow -jk_0h(x_{s1}')(n_y^i - n_y')$ and/or $\exp[jk_0h(x_{s2}')(n_y^f - n_y')] - 1 \rightarrow jk_0h(x_{s2}')(n_y^f - n_y')$. The expression for the diffuse double-scatter field does not contain the zero-order term.[20]

APPENDIX B

On deriving the shadow function associated with the multiple-scatter event $[1 - P_2(|n_y'|)][1 - P_2(|n_y''|)]$, we assumed here, as in the earlier studies by Sancer[17] and Smith,[18] that the shadow function is statistically independent of the height-dependent phase terms in the field expressions. Strictly speaking, even in the high-frequency limit (where the phase term is shown to be proportional to the slopes of the rough surface[17,28]), the shadow function is not statistically independent of the phase term, since the heights and the slopes are correlated, particularly at high frequencies.[10] Furthermore, it is necessary for the double-scatter cross sections to satisfy reciprocity and continuity for all incident and scatter angles. To this end, shadowing associated with the single-scatter event is expressed as the product $P_2(-n_y^i)P_2(n_y^f)$, where $P_2(\hat{n}^i)$is the probability that a point on the surface is illuminated by a plane wave in the direction of the unit vector $\hat{n}^i$ and visible by an observer in the direction of the unit vector $\hat{n}^f$.[18]

For the multiple-scatter event the unit vector $\hat{n}'$, for example, is both in the direction of the scattered wave at point 1′ and in the direction of the incident wave at point 2′. Thus, in order to account for scattering at point 1′, we represent by $1 - P_2(n_y')$ the probability that the scattered wave emerging from point 1′ in the direction $\hat{n}'$ intersects the surface, and, in order to account for scattering at point 2′, we represent by $1 - P_2(-n_y')$ the probability that an incident wave in the direction $\hat{n}'$ intersects the surface at point 2′. Now, since $P_2(\alpha) = 0$ when α is negative, it follows that $[1 - P_2(n_y')][1 - P_2(-n_y')] = 1 - P_2(|n_y'|)$. This result ensures reciprocity. It should also be pointed out that the full-wave slope-dependent surface element scattering coefficients $D^P[\hat{n}^f, \hat{n}^i)$ intrinsically account for self-shadow through the unit step functions $S(\hat{n}^f \cdot \hat{n})$ and $S(-\hat{n}^i \cdot \hat{n})$ (see Appendix A).

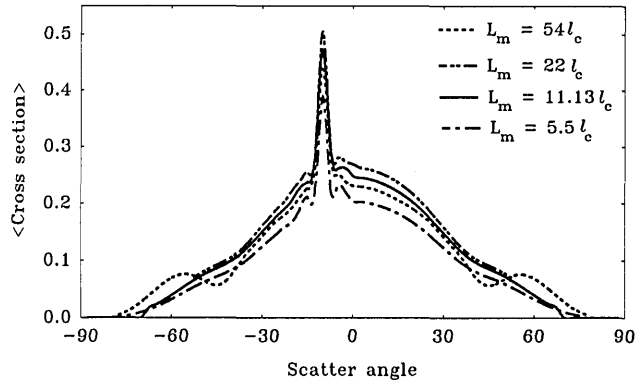

Fig. 24. Vertically polarized double-scatter average cross sections plotted versus scatter angle ($\equiv \theta^f \cos \phi^f$ for $\phi^f = 0, \pi$ and $\phi^i = 0$) for different values of double-scatter mean path L_m and for $\theta^i = 10°$, $\beta = 356.128$, $\langle h_x^2 \rangle = 0.508$, $\lambda = 1.152$ μm, and $\epsilon_r = -62.787 - j4.948$.

APPENDIX C

In this paper we used the expression derived by Beckmann[31] for the mean duration of a fade, $T^-(h)$, to obtain the double-scatter mean path L_m. This quantity depends on the height h (level of signal[31]). For a Gaussian surface height probability-density function the mean duration of the fade, $T^-(h)$, is[22,31]

$$T^-(h) = \frac{\pi}{\Omega} \exp(h^2/2\langle h^2 \rangle)\left\{1 + \operatorname{erf}\left[\frac{h}{(2\langle h^2 \rangle)^{1/2}}\right]\right\}, \quad \text{(C1)}$$

where $\Omega = \sqrt{2}/l_c$ and l_c is the correlation length. For a typical (sinusoidal) depression (valley), Ishimaru and Chen[22] assume that $L_m = T^-[h = (2\langle h^2 \rangle)^{1/2} = 11.13 l_c]$. This value is used in the illustrative examples.

Since the width of a typical depression (or a valley) on the surface is a random variable (say, L_v) with mean value L_m, in principle it is necessary to take the statistical average of the results developed in Section 2 over the random variable L_v. However, as we show in Fig. 24, the numerical results for the double-scatter cross sections are insensitive to the values of L_m over a wide range of values about $L_m = 11.13 l_c$. Thus, if the standard deviation of L_v is small compared with that of L_m, this statistical average of the results presented in Section 3 are not significantly different from those given for $L_m = 11.13 l_c$.

ACKNOWLEDGMENTS

The computations were conducted at the Cornell National Supercomputer Facility supported by the National Science Foundation. This research was partially supported by the U.S. Army Research Office and the Center for Electro-Optics at the University of Nebraska—Lincoln.

REFERENCES AND NOTES

1. E. R. Mendez and K. A. O'Donnell, "Observations of depolarization and backscattering enhancement in light scattering from Gaussian random surfaces," Opt. Commun. **61,** 91–95 (1987).
2. K. A. O'Donnell and E. R. Mendez, "Experimental study of scattering from characterized random surfaces," J. Opt. Soc. Am. A **4,** 1194–1205 (1987).
3. P. H. A. Ishimaru, J. S. Chen, P. Phu, and K. Yoshitomi, "Numerical, analytical, and experimental studies of scattering from very rough surfaces and backscattering enhancement," Waves Random Media **1,** S91–S107 (1991).
4. Workshop on Enhanced Backscatter at Boulder, Colo., on January 10–11, 1992, conducted by the U.S. Army Research Office, P.O. Box 12211, Research Triangle Park, N.C. 27709.
5. M. E. Knotts, T. R. Michel, and K. A. O'Donnell, "Comparison of theory and experiment in light scattering from a randomly rough surface," J. Opt. Soc. Am. A **10,** 928–941 (1993).
6. M. El-Shenawee, "Full wave multiple scattering and depolarization of electromagnetic fields from rough surfaces," Ph.D. dissertation (University of Nebraska—Lincoln, Lincoln, Neb., 1991).
7. E. Bahar and M. El-Shenawee, "Full wave multiple scattering from rough surfaces," presented at the IEEE APS International Symposium and URSI Radio Science Meeting, Dallas, Texas, 1990.
8. E. Bahar and M. El-Shenawee, "Use of supercomputers to evaluate singly and doubly scattered electromagnetic fields from rough surfaces," IEEE Trans. Mag. **27,** 4287–4290 (1991).
9. E. Bahar and M. El-Shenawee, "Multiple scattering from random distributions of individual rough surface scatterers," presented at the IEEE APS International Symposium and URSI Radio Science Meeting, Chicago, Ill., 1992.
10. E. Bahar, "Full wave analysis for rough surface diffuse, incoherent radar cross sections with height-slope correlations included," IEEE Trans. Antennas Propag. **39,** 1293–1304 (1991).
11. E. Bahar and M. El-Shenawee, "Full wave multiple scattering from one dimensional random rough surfaces and high frequency stationary phase approximations," presented at the IEEE Antennas and Propagation Society International Symposium, Ann Arbor, Mich., 1993.
12. E. Bahar and M. El-Shenawee, "Multiple scattering from one dimensional random rough surfaces—full wave solutions," presented at the Progress in Electromagnetics Research Symposium, Pasadena, Calif., 1993.
13. E. Bahar and M. El-Shenawee, "High frequency approximations to multiple scatter that exhibit enhanced backscatter," presented at the 1993 International Geoscience and Remote Sensing Symposium, Tokyo, Japan, 1993.
14. E. Bahar, "Radio wave propagation in stratified media with nonuniform boundaries and varying electromagnetic parameters: full wave analysis," Can. J. Phys. **50,** 3132–3142 (1972).
15. L. M. Brekhovskikh, *Waves in Layered Media* (Academic, New York, 1960).
16. E. Bahar, "Generalized Fourier transform for stratified media," Can. J. Phys. **50,** 3123–3131 (1972).
17. M. I. Sancer, "Shadow-corrected electromagnetics scattering from a randomly rough surface," IEEE Trans. Antennas Propag. **AP-17,** 577–585 (1969).
18. B. G. Smith, "Geometrical shadowing of a random rough surface," IEEE Trans. Antennas Propag. **AP-15,** 668–671 (1967).
19. E. Bahar and B. S. Lee, "Full wave solutions for rough surface bistatic radar cross sections—comparison with small perturbation, physical optics, numerical and experimental results," Radio Sci. **29,** 407–429 (1994).
20. S. O. Rice, "Reflection of electromagnetic waves from slightly rough surfaces," Commun. Pure Appl. Math. **4,** 351–378 (1951).
21. A. R. McGurn, A. A. Maradudin, and V. Celli, "Localization effects in the scattering of light from a randomly rough grating," Phys. Rev. B **31,** 4866–4871 (1985).
22. A. Ishimaru and J. S. Chen, "Scattering from very rough surfaces based on the modified second order Kirchhoff approximation with angular and propagation shadowing," J. Acoust. Soc. Am. **88,** 1877–1883 (1990).
23. A. A. Maradudin and E. R. Mendez, "Enhanced backscattering of light from weakly rough, random metal surfaces," Appl. Opt. **32,** 3335–3343 (1993).
24. R. T. Deck and H. J. Simon, "Simple diffractive theory of enhanced backscattering," J. Opt. Soc. Am. B **10,** 1000–1005 (1993).
25. E. Bahar and M. El-Shenawee, "Numerical method to compute TE and TM multiple scatter from rough surfaces exhibiting backscatter enhancement," presented at the Computation of Electromagnetic Fields, Miami, Fla., 1993.
26. Y. Kuga, J. S. Colburn, and P. Phu, "Millimeter-wave scattering from one dimensional surfaces of different surface correlation functions," Waves Random Media (to be published).
27. P. Beckmann and A. Spizzichino, *The Scattering of Electromagnetic Waves from Rough Surfaces* (Macmillan, New York, 1963).
28. D. E. Barrick, "Relationship between slope probability density function and the physical optics integral in rough surface scattering," Proc. IEEE **56,** 1728–1729 (1968).
29. E. Bahar and Y. F. Li, "Statistical characterization of random rough surfaces using the tilt modulation of the backscattered radar cross section—full wave approach," presented at the International Geoscience and Remote Sensing Symposium, College Park, Md., 1990.
30. A. M. Mood, F. A. Graybill, and D. C. Boes, *Introduction to the Theory of Statistics* (McGraw-Hill, New York, 1974).
31. P. Beckmann, *Elements of Applied Probability Theory* (Harcourt, Brace & World, New York, 1968), p. 173.
32. E. Bahar, "Full-wave solutions for the depolarization of the scattered radiation fields by rough surfaces of arbitrary slope," IEEE Trans. Antennas Propag. **AP-29,** 443–454 (1981).
33. E. Bahar and M. A. Fitzwater, "Depolarization and backscatter enhancement in light scattering from random rough surfaces: comparison of full-wave theory with experiment," J. Opt. Soc. Am. A **6,** 33–43 (1989).